Geochemical and radiogenic isotope records of the Weissert Event in south Tethyan sediments

M. Shmeit, C. Chauvel, F. Giraud, E. Jaillard, S. Reboulet, M. Masrour, J E Spangenberg, A. El-Samrani

Accepted Manuscript

Journal of the Geological Society

Geochemical and radiogenic isotope records of the Weissert Event in south Tethyan sediments

M. Shmeit, C. Chauvel, F. Giraud, E. Jaillard, S. Reboulet, M. Masrour, J.E. Spangenberg & A. El-Samrani

DOI: https://doi.org/10.1144/jgs2022-023

To access the most recent version of this article, please click the DOI URL in the line above. When citing this article please include the above DOI.

Received 14 February 2022
Revised 10 October 2022
Accepted 29 November 2022

Supplementary material at https://doi.org/10.6084/m9.figshare.c.6333040

Geochemical and radiogenic isotope records of the Weissert Event in south Tethyan sediments

M. Shmeit[1,3*], C. Chauvel[1,2], F. Giraud[1], E. Jaillard[1], S. Reboulet[4], M. Masrour[5], J.E. Spangenberg[6], A. El-Samrani[3]

1. Univ. Grenoble Alpes, Univ. Savoie Mont Blanc, CNRS, IRD, Univ. Gustave Eiffel, ISTerre, 38000 Grenoble, France

2. Université de Paris, Institut de Physique du Globe de Paris, CNRS, F-75005 Paris, France

3. Lebanese University, Doctoral School of Science and Technology, Laboratory of Geosciences Georesources and Environment L2GE, EDST/PRASE, Beirut, Lebanon

4. Univ Lyon, UCBL, ENSL, UJM, CNRS, LGL-TPE, F-69622, Villeurbanne, France

5. Université Ibn Zohr, Faculté des Sciences, Département de Géologie, BP 8106, Cité Dakhla, Agadir, Morocco

6. University of Lausanne, Institute of Earth Surface Dynamics (IDYST), CH-1015 Lausanne, Switzerland

Ordic ID: M.S., 0000-0003-0291-4968; C.C., 0000-0002-3959-4665; F.G., 0000-0002-4732-4737; S.R., 0000-0002-7232-8596; M.M., 0000-0001-6821-9023; J.E.S., 0000-0001-8636-6414; A.E.S, 0000-0002-2654-4212

Authors emails: majd.homaidan-shmeit@u-bourgogne.fr; chauvel@ipgp.fr; fabienne.giraud-guillot@univ-grenoble-alpes.fr; etienne.jaillard@univ-grenoble-alpes.fr; stephane.reboulet@univ-lyon1.fr; moussamasrour5@gmail.com; jorge.spangenberg@unil.ch; antoineelsamrani@ul.edu.lb

*Corresponding author currently at: Biogéosciences, UMR 6282 CNRS, Université Bourgogne Franche-Comté, 6 Bvd Gabriel, 21000 Dijon, France. E-mail address: majd.homaidan-shmeit@u-bourgogne.fr (M. Shmeit).

ABSTRACT:

The Cretaceous marine sedimentary record is characterized by time intervals rich in organic matter correlating with positive carbon-isotope excursions, often called oceanic anoxic events. The Weissert Event corresponds to the first such event in the Cretaceous during the Valanginian stage. The associated palaeoenvironmental perturbations which include increasing marine surface-water primary productivity are hypothesized to be triggered by volcanic activity from large igneous provinces, and the source of nutrients is not well-constrained (continental runoff *vs.* oceanic upwelling). We present isotope ratios of Pb, Sr and Nd together with concentrations of major and trace elements for sediments coming from the central Moroccan margin to test these hypotheses. We demonstrate that the nutrient input was dominated by continental weathering. Also, the source of sedimentary material remained stable during the Valanginian interval and it originated in an old source, probably the African Sahara region. The radiogenic isotope signatures do not show a significant contribution of volcanic products from any known Valanginian large igneous province to the geochemical budget of sediments deposited on the central Moroccan margin. While this does not preclude an impact of volcanic activity on the composition of seawater, it demonstrates that erupted volumes were not sufficient to affect the deposited sediments.

Supplementary material: A supplementary table (Microsoft Excel) is attached with the submission. It contains three sheets: (1) “Central Moroccan Margin”, the analytical data generated and analysed during this study; (2) “Fig.8 Data - LIPs”, the data of known Valanginian large igneous provinces used for comparison; and (3) “Fig.9 & S5 Data - source areas”, the data of potential surrounding source areas used for comparison.

The Cretaceous marine sedimentary record is characterized by several positive carbon-isotope excursions (CIEs) corresponding to perturbations in the global carbon-cycle (Scholle and Arthur, 1980; Weissert et al., 1998). These are mainly explained by enhanced marine and terrestrial primary productivity and/or enhanced preservation of organic matter (Scholle and Arthur, 1980; Weissert, 1989; Kump and Arthur, 1999). Positive CIEs are often associated with records of widespread organic-rich oceanic sediments termed as "Oceanic Anoxic Events" (OAEs, Schlanger and Jenkyns, 1976; Scholle and Arthur, 1980). The Valanginian stage (137.7–132.6 Ma; Gale et al., 2020) records the first positive CIE of the Cretaceous and is named the Weissert OAE (Lini et al., 1992; Weissert et al., 1998; Erba et al., 2004). However, its expression as an OAE is doubted due to the absence of significant and widespread organic-rich layers (Westermann et al., 2010; Kujau et al., 2012). The most significant in the Tethyan Realm being the centimetric "Barrande" layers (1.9 – 3.7 % TOC), observed prior to the Valanginian positive CIE in the Vocontian basin (SE France) (Reboulet et al., 2003).

The positive CIE corresponding to the "Weissert Event" is observed in a wide range of geographic locations such as the Tethys, Atlantic, Pacific, Boreal Realm and the Southern Hemisphere (Hennig et al., 1999; Bartolini, 2003; Price and Mutterlose, 2004; Sprovieri et al., 2006; McArthur et al., 2007; Aguirre-Urreta et al., 2008; Bornemann and Mutterlose, 2008; Charbonnier et al., 2013; Price et al., 2018). Following Martinez et al (2015), the onset of the Valanginian CIE is recorded at 135.22 ±1.0 Ma, and it is characterized by three phases: (1) rapid $\delta^{13}C_{carb}$ increase lasting 0.60 myr, (2) stable $\delta^{13}C_{carb}$ values with a duration of 1.48 myr, and (3) smooth decrease in $\delta^{13}C_{carb}$ lasting 3.77 myr. This CIE is recorded in marine carbonates and organic matter (Lini et al., 1992; Channell et al., 1993; Gréselle et al., 2011; Aguado et al., 2018), and in terrestrial fossil plants (Gröcke et al., 2005) implying a perturbation in both the oceanic and atmospheric carbon reservoirs.

The Weissert Event is associated with a warm and humid climate (Lini et al., 1992; Charbonnier et al., 2020), enhanced marine primary productivity (Bersezio et al., 2002; Bartolini, 2003; Erba and Tremolada, 2004; Duchamp-Alphonse et al., 2007; Bornemann and Mutterlose, 2008; Mattioli et al., 2014) and a biocalcification crisis in platform and pelagic settings (Channell et al., 1993; Weissert et al., 1998; Wortmann and Weissert, 2000; Erba and Tremolada, 2004; Föllmi et al., 2006). Two main hypotheses explain eutrophication (i.e., nutrient input) of the marine environment in proximal and distal marine settings. Intensification of the hydrological cycle is suggested to cause higher detrital and nutrient input in proximal settings close to fluvial influx (Lini et al., 1992; Jenkyns, 2003; Erba et al., 2004). In contrast, nutrient input in pelagic settings is often explained by the introduction of nutrients from oceanic upwelling (Arthur et al., 1990; Weissert et al., 1998; Jenkyns, 2010; Föllmi, 2012). Such hypotheses proposed for the fertilization of the ocean need to be examined for the Weissert Event.

The triggering conditions causing the environmental perturbations of the Weissert Event are tentatively linked with extensive volcanism from the Paraná-Etendeka large igneous province (LIP; Weissert et al., 1998; Erba et al., 2004; Charbonnier et al., 2017) or the Comei-Bunbury LIP (Zhu et al., 2009). Radiometric ages of basalts from the aforementioned LIPs cluster around 135.5–126 Ma (Liu et al., 2015; Almeida et al., 2018; Baksi, 2018; Rocha et al., 2020; Bacha et al., 2021), likely postdating the onset of the Valanginian positive CIE (135.22 ±1.0 Ma, Martinez et al., 2015). Previous studies used Pb isotopes from ODP (ocean drilling program) Leg 185 Hole 1149B (western Pacific) to demonstrate a link between the Weissert Event and the Paraná-Etendeka LIP (Chavagnac et al., 2008; Peate, 2009). However, constraints provided by Sr and Nd isotopes are not necessarily consistent with such interpretation and the number of Valanginian samples showing a Pb isotopic shift is very low.

In this study, we report major and trace element concentrations and radiogenic isotope ratios of Pb, Sr and Nd in Valanginian carbonate sediments from two stratigraphic successions on the central Moroccan margin. Comparing data obtained on sediments from an onshore section (Zalidou; Essaouira-Agadir Basin) and an offshore Deep Sea Drilling Project succession (DSDP Leg 50 Hole 416A; east Atlantic) allows investigation of the geochemical similarities and differences between a proximal and a distal site on the same margin. In both sites, temporal geochemical variations are constrained by an accurate chronostratigraphic framework allowing us to establish whether changes occur before, during or after the Weissert Event. Ultimately, the aim of this study is to: (a) determine whether the source of nutrients (i.e., eutrophication) is continental runoff, oceanic upwelling or both and (b) search for a volcanic contribution in the sediments, a feature that would support a volcanic origin for the Weissert Event.

Geological setting

The Essaouira-Agadir Basin faces the eastern Atlantic margin and is located in the western High Atlas in Morocco (9°55' to 9°20' W, 30°30' to 31°05' N) (Fig. 1). The Essaouira-Agadir Basin extends offshore until the western limit of the continental margin and constitutes part of the present-day Atlantic passive margin (Frizon de Lamotte et al., 2008). Consequently, the geologic evolution of the passive margin controlled that of the basin itself (Ellouz et al., 2003). Post-rift sedimentation along with thermal subsidence started in the middle Jurassic and an eustatic transgression gave way to extended marine sedimentation during the Early Cretaceous (Berriasian to early Hauterivian; Piqué et al., 1998; Hafid et al., 2008; Frizon de Lamotte et al., 2009). During the Early Cretaceous, the basin corresponded to a temperate platform on the south Tethyan margin between palaeo-latitudes ~15°N and ~22°N (Fig. 2).

Sedimentary rocks of Valanginian age (137.7–132.6 Ma) were sampled from two different geological successions on the central Moroccan margin, one being onshore and proximal (the

Zalidou section) and the other being offshore and distal (DSDP Hole 416A) (Fig. S1). Both geological successions have a well-constrained biostratigraphy (ammonites for the onshore succession, and calcareous nannofossils) and chemostratigraphy (carbon isotopes) allowing to identify the Weissert Event (Reboulet et al., 2022; Shmeit et al., 2022). The combination of the two successions allowed investigation of how the geochemical signature in a proximal setting close to river-influence compares to that in a distal setting close to possible oceanic upwelling (Price et al., 1995; Poulsen et al., 1998).

The Zalidou section

The section is located onshore ~100 km north of Agadir city (30°54'23"N; 9°39'48"W) (Fig. 1b). The rocks of Valanginian age are particularly well exposed and the lithostratigraphy and biostratigraphy (ammonites and calcareous nannofossils) are presented in Reboulet et al. (2022) (Fig. S2). Briefly, the section is dated from the late Berriasian (older than 137.7 Ma, GTS 2020) to earliest Hauterivian (younger than 132.6 Ma, GTS 2020) and consists of an alternation of limestone and marlstone during the Valanginian stage (Fig. S2). The lower Valanginian is dominated by marlstone and thin limestone beds, whereas in the upper Valanginian sandy deposits (sandy marlstone, sandy limestone and calcareous sandstone) become more common. Traces of pyrite are observed suggesting that reducing conditions occurred during the lower Valanginian; however, no organic-rich facies were detected. The Weissert Event interval is identified from the lower part of the *K. inostranzewi* to the upper part of the *N. peregrinus* ammonite standard zones (upper NK3A to upper NK3B, and upper CC3b to upper CC4a calcareous nannofossil subzones) (Fig. S2) (Reboulet et al., 2022; Shmeit et al., 2022).

The DSDP Leg 50 Hole 416A drill core

The offshore succession was drilled ~238 km NW of Zalidou (32°50'10.7"N; 10°48'03.6"W), at a water depth of 4201 m on the east Atlantic Ocean (Lancelot et al., 1980) (Fig. S1). The

Valanginian interval is identified using calcareous nannofossils between 1542 and 1119 mbsf (meters below seafloor; from Cores 49 to 9) (Čepek and Gartner, 1980; Shmeit et al., 2022), but the uppermost Valanginian is missing (Shmeit et al., 2022). The lithology is described in Lancelot et al. (1980). Briefly, the lithological unit VII (1624 to 1430 mbsf; Fig. S2) is characterized by alternation of terrigenous and carbonate-rich turbidite cycles. The terrigenous cycles consist of fine-grained sandstone, siltstone and mudstone; whereas, the carbonate-rich cycles consist of quartz-rich calcarenite, micritic limestone, siltstone and marlstone. The overlying lithological unit VI (1430 to 880 mbsf) is characterized by distal terrigenous turbidites and differs from Unit VII by the absence of micritic limestones. The cycles in lithological unit VI consist of fine sandstone, siltstone, silty-mudstone along with calcareous mudstone and marlstone. The Weissert Event interval is identified from the upper NK3A to NK3B and CC3b to CC4a calcareous nannofossil subzones (from 1303 to 1122 mbsf; Fig. S2) but part of the Event is probably missing (Shmeit et al., 2022).

Materials and methods

We selected twenty samples from the Valanginian in Zalidou section and forty-eight from DSDP Hole 416A (Fig. S2). The Zalidou samples correspond to marlstone and argillaceous-limestone. For Hole 416A, samples were collected in the finest parts of the turbiditic cycles corresponding to marlstone and mudstone. Such fine-grained lithologies were selected to minimize geochemical changes due to different rock types that would potentially overprint those due to source/sedimentation changes. The Zalidou samples have $CaCO_3$ content of ~40 %, and Hole 416A samples between 8 and 50% (Shmeit et al., 2022; Supplementary Table). Due to the scarcity of available samples in the upper Valanginian of Hole 416A, we chose samples with the highest possible $CaCO_3$ content although it was low (<10 %). All samples were finely crushed in an agate mortar for the subsequent elemental and isotopic analyses.

Major and trace elements

Major elements and loss on ignition were measured by the CNRS Service d'Analyse des Roches et des Minéraux (SARM) in Nancy, France. Rock samples were digested using alkali fusion, and major element analyses were done by flow injection inductively coupled plasma mass spectrometry (ICP-MS) following Carignan et al. (2001). Accuracy was assessed based on international reference materials (BR, AN-G, UB-N, DR-N and GH; Carignan et al., 2001). Complete duplicate analysis of one of our samples demonstrates a reproducibility better than 5 % (Supplementary Table). Also, the chemical index of alteration (CIA) was calculated using the molecular proportions of Al, Ca, Na and K oxides while also correcting the molar proportion of CaO for phosphate and carbonate. This correction is needed for carbonate sediments to restrict the molar proportion of CaO to that derived from silicate minerals (see Bomou et al., 2013; and references therein).

Trace element concentrations were measured at the IPGP (Institut de Physique du Globe de Paris) Paris, France. The methods used were similar to those described in Chauvel et al. (2011), with slight modifications. About 100 mg of each sample was dissolved in concentrated HNO_3:HF using Parr bombs maintained at 150^{o}C for over two weeks. The only exceptions were the three basalt reference materials (BHVO-2, BR-24 and BE-N) digested in Savillex Teflon beakers because they do not contain refractory minerals. After dissolution, samples were diluted using 0.5M HNO_3 plus traces of HF to reach a dilution factor of 10000. A 5 ppb indium standard was added to all samples prior to measurement on an Agilent 8900 ICP-MS. Except for low masses ^{7}Li, ^{9}Be and ^{11}B, all masses were measured in collision mode with a 5 ml min^{-1} He flux in the collision reaction cell to remove polyatomic interferences. The international reference material BE-N was used to calibrate the signal (external calibration) and was run every 5-6 samples during the entire sequence. The procedural blanks were negligible. The accuracy of our data as evaluated from analyses of reference rock materials (BHVO-2 and BR-24) is generally better than 5 % (Supplementary Table). The

precision was assessed from complete duplicate analyses of three samples that reproduce within 5 % for most elements (Supplementary Table).

Radiogenic isotopes (Pb, Sr and Nd)

Chemical separations and isotopic measurements were done at the IPGP. Methods generally follow those described in Chauvel et al. (2011) after the dissolution of approximately 50 mg of rock powder in Savillex Teflon beakers at 125^{o}C for ten days. Procedural blanks (n= 12) were low (Pb <54 pg, Sr <100 pg and Nd <86 pg), but there were two exceptions: one Sr blank at 770 pg and one Nd blank at 1800 pg. These two high values remain negligible relative to the quantity of element in the samples and correspond to 0.016 % and 1.05 % of the mass isolated from the least concentrated samples for Sr and Nd, respectively. Pb, Sr and Nd isotopic ratios were measured on a Multi-Collector ICP-MS (Thermo scientific Neptune plus) equipped with an Apex IR introductory system. Cones used for lead and strontium were a Jet sampler with an H skimmer, and for neodymium a Jet sampler with an X skimmer. The sample flow rate was at 50 µl min^{-1}; sample measurement, including the wash and uptake time, was 10 min/sample. For Nd, N_2 gas was introduced in the Apex IR system at 4 bars pressure to reduce the oxides of Nd, which could form in the plasma and interfere with the signal.

Measured strontium and neodymium isotope ratios were normalized to $^{88}Sr/^{86}Sr = 0.1194$ and $^{146}Nd/^{144}Nd = 0.7219$ (O'Nions et al., 1979). For lead measurements, the samples were spiked with thallium (5 ppb) and normalized to $^{205}Tl/^{203}Tl$: 2.38714 (White et al., 2000). International reference materials (NBS 981 Pb, NBS 987 Sr and AMES Rennes Nd) were measured every four samples, and the average isotopic ratio of the session was used to correct for the bias relative to values published by Jochum et al. (2011) for Pb, by Thirlwall (1991) for Sr and by Chauvel et al. (2011) for Nd. Isotopic ratios measured on complete duplicate analyses of five

samples and two dissolutions of the AGV-2 geochemical reference demonstrate that both the reproducibility and the accuracy are excellent (Supplementary Table).

The initial isotope ratios of Pb, Sr and Nd were calculated at 135 Ma to correct for radiogenic decay (Equation 1; Supplementary Table).

$$\left(\frac{D}{D'}\right)_{present-day} = \left(\frac{D}{D'}\right)_{initial} + \left(\frac{P}{D'}\right)_{initial}\left(e^{\lambda t} - 1\right) \quad (1)$$

with D: radiogenic daughter isotope, D': stable isotope of the same element, P: radioactive parent isotope, λ: decay constant and t: time in years.

Results

Major elements

The major element contents of Zalidou and Hole 416A samples are reported in Supplementary Table. The average Al_2O_3 content is higher in Hole 416A (15 ±7 wt%) than in Zalidou (9 ±5 wt.%) (Fig. 3). The errors correspond to variability between samples, calculated as two times the standard deviation of the mean. In contrast, the average SiO_2 content is slightly higher in the Zalidou samples (47 ±15 wt%) than in Hole 416A samples (43 ±17 wt%). The CaO is comparable between both successions but shows larger variation in Hole 416A (avg. 11 ±15 wt%) than in Zalidou (avg. 17 ±10). The studied sediments from Zalidou lie in the middle of a "triangular" field defined by three end-members of oceanic sediment composition (i.e., silica-rich, clay and carbonate) while most of the Hole 416A samples define a trend between clay and carbonate (Fig. 3).

Stratigraphic variations in the SiO_2 and CaO contents (wt.%) at Zalidou show a stable trend during the entire studied interval (Fig. 4). The Al_2O_3 content shows possibly higher values (12 ±6 wt.%) in the upper part of the Weissert Event between 25.05 and 32.8 m, compared with the rest of the succession (9 ±5 wt.%) (Fig. 4). Also, the calculated CIA is slightly higher (74 ±4) in the same interval compared with the rest of the succession (68 ±6). At Hole 416A, the SiO_2 content is steady throughout the studied interval (Fig. 4). The Al_2O_3 content increases

from 11 ±2 wt.% before the Weissert Event (NK3A and upper CC3a to lower CC3b nannofossil subzones) to 16 ±7 wt.% during it (upper NK3A to NK3B and upper CC3b to CC4a nannofossil subzones). The CaO content is low (7 ±8 wt.%) within the Weissert Event between 1280.7 and 1187.9 mbsf (upper NK3A to NK3B and upper CC3b to CC4a nannofossil subzones), compared with the rest of the succession (19 ±15 wt.%) (Fig. 4). Lastly, the CIA does not signficantly vary.

Trace elements

Figure 5 shows the concentrations in Zalidou and Hole 416A of Al_2O_3 *vs.* selected trace elements representing different oceanic sediment end-members. Lithium, which is contained in fine-grained clays, is higher in Hole 416A (avg. 87 ±42 ppm) compared with Zalidou (avg. 46 ±37 ppm) (Fig. 5a). Similarly, this applies to other elements contained in clays (e.g., Cs and Rb; Supplementary Table). The REE contents, whose budget is mainly controlled by the abundance of clays, are slightly higher in Hole 416A than in Zalidou. For example, the concentration of Nd is higher in Hole 416A (avg. 33 ±17 ppm) compared with Zalidou (avg. 25 ±2 ppm) (Fig. 5b). Strontium, which substitutes Ca in calcium carbonate minerals, is higher and more variable in Hole 416A (avg. 407 ±239 ppm) compared with Zalidou (avg. 302 ±215 ppm) (Fig. 5c). Lastly, the high field strength elements (HFSE), mainly carried by heavy minerals present in the coarse-grained detrital sands, are significantly higher in Zalidou than in Hole 416A (Supplementary Table). For example, the Zr concentration is on average 302 ±217 ppm in the former section against a lower concentration of 137 ±63 in the latter (Fig. 5d).

Stratigraphic variations, at Zalidou, in the trace elements contained in clays and coarser grain detrital materials (Li and Nd) are stable throughout the studied interval (Fig. 4). Strontium, possibly representing a carbonate component, is also stable. The Zr concentration is consistently low (178 ±87 ppm) in the upper part of the Weissert Event between 25.05 and

32.8 m, compared with the rest of the succession (346 ±176 ppm) (Fig. 4). This corresponds to the time interval when Al_2O_3 contents are higher (*O. nicklesi* ammonite Subzone, NK3B and CC4a nannofossil subzones; Fig. 4). At Hole 416A, the concentration of Li increases from 61 ±7 ppm before the Weissert Event to 90 ±40 ppm after it (Fig. 4); this corresponds to the time interval when Al_2O_3 contents also increase (upper NK3A to NK3B and upper CC3b to CC4a nannofossil subzones). The concentration of Nd is steady during the studied interval, although it is variable during the Weissert Event (Fig. 4). The concentrations of Sr and Zr are steady on average during the studied interval.

Radiogenic isotopes

The initial (i) and measured (m) isotopic ratios display similar stratigraphic trends, and the former are consistently slightly lower than the latter (Fig. 6). In Zalidou, Pb isotopic ratios are stable during the entire Valanginian stage ($^{206}Pb/^{204}Pb_{(i)}$: avg. 18.61 ±0.16 and $^{208}Pb/^{204}Pb_{(i)}$: 38.68 ±0.26, 2σ) except for the $^{207}Pb/^{204}Pb_{(i)}$, which potentially increases slightly from 15.678 ±0.004 (2σ) before the Weissert Event to 15.683 ±0.011 (2σ) during the Event, and to 15.685 ±0.006 (2σ) after it. The Sr isotope ratios are also stable throughout the studied interval (avg. 0.710 ±0.001, 2σ). However, the $^{143}Nd/^{144}Nd_{(i)}$ are less variable (0.51190 ±0.00002, 2σ) before the Weissert Event and in its lower part, than in the rest of the succession (0.51190 ±0.00004, 2σ) (Fig. 6). Two "outliers" have different Pb initial isotope ratios in the Zalidou section (Za 51b: 28.95 m and Za 56a: 40.6 m; Fig. 6). Sample Za 51b has a low $^{206}Pb/^{204}Pb_{(i)}$ and a high $^{208}Pb/^{204}Pb_{(i)}$ due to its high U/Pb and low Th/Pb ratios (Supplementary Table). Sample Za 56a has a low $^{208}Pb/^{204}Pb_{(i)}$ because of its high Th/Pb ratio. We suspect that these anomalous ratios are due to recent events and are unrelated to the original contents, resulting in an overcorrection with age. In Hole 416A, Pb isotopic ratios are steady during the Valanginian stage ($^{206}Pb/^{204}Pb_{(i)}$: avg. 18.68 ±0.15; $^{207}Pb/^{204}Pb_{(i)}$: 15.69 ±0.02; $^{208}Pb/^{204}Pb_{(i)}$: 38.73 ±0.15, 2σ). The Sr isotopic ratios are highly variable (avg. 0.7106 ±0.0027, 2σ) and do

not show any significant trend. The Nd isotopic ratios are moderately constant (avg. 0.51190 ±0.00007, 2σ). The $^{143}Nd/^{144}Nd_{(i)}$ show minor variations (0.51187 ±0.00003, 2σ) during the Weissert Event (between 1263 and 1188 mbsf; upper NK3A-lower NK3B and upper CC3b nannofossil subzones) than during the rest of the studied time-interval (0.51191 ±0.00007, 2σ).

The $^{206}Pb/^{204}Pb_{(i)}$ and $^{207}Pb/^{204}Pb_{(i)}$ are similar in the two sites (Fig. 7a). However, the $^{208}Pb/^{204}Pb_{(i)}$ are slightly higher in Hole 416A than in Zalidou, such that the majority of Hole 416A samples have $^{208}Pb/^{204}Pb_{(i)}$ >38.75 while Zalidou samples have ratios <38.75 (Fig. 7b). The $^{87}Sr/^{86}Sr_{(i)}$ isotopic ratios are on average slightly higher and more variable in Hole 416A than in Zalidou, some samples from Hole 416A have $^{87}Sr/^{86}Sr_{(i)}$ >0.7106 (Fig. 7c). In contrast, all samples from Zalidou have ratios <0.7106. Finally, the $^{143}Nd/^{144}Nd_{(i)}$ ratios are similar in both successions (Fig. 7d).

Discussion

The positive carbon isotope excursion (CIE) corresponding to the Weissert Event (Valanginian stage, 137.7–132.6 Ma) is mainly interpreted as the consequence of enhanced marine primary productivity (Lini et al., 1992; Bartolini, 2003; Erba et al., 2004). Multiple micropalaeontological (e.g., Bersezio et al., 2002; Duchamp-Alphonse et al., 2007; Bornemann and Mutterlose, 2008; Mattioli et al., 2014) and geochemical studies (e.g., Plank et al., 2000; Bartolini, 2003; Morales et al., 2015) support increasing marine primary productivity and fertility during the Valanginian stage.

An increase in marine primary productivity requires enhanced nutrification, and two main hypotheses exist: higher continental weathering rates or intensified oceanic upwelling (Lini et al., 1992; Föllmi et al., 1994; Erba et al., 2004). The two processes would have different impacts in proximal and distal marine settings. Thus, comparing the time evolution of the two types of settings could help understand the cause(s) of increasing productivity. Enhanced

continental weathering and hydrolyzing conditions are demonstrated during the Valanginian stage from clay-mineral assemblages (Westermann et al., 2013; Charbonnier et al., 2020), spore-pollen ratios (Kujau et al., 2013) and sediment-enrichments in continentally sourced elements (Al, Mn, Fe and P; Van De Schootbrugge et al., 2003; Kuhn et al., 2005; Duchamp-Alphonse et al., 2007; Morales et al., 2015). Continental weathering ultimately increases nutrient input in proximal marine settings close to fluvial discharge. Thereby, substantial nutrient input from the continent would result in a crustal geochemical signature on the central Moroccan margin sediments, particularly in the proximal setting (Zalidou) which is closer to river input. In contrast, the upwelling of nutrient-rich deep waters should increase nutrient levels in pelagic settings (Bartolini, 2003; Erba et al., 2004; Föllmi, 2012). Existing evidence include abundance peaks in the radiolarian taxa *Pantanellium* in the Tethys and the Pacific (Jud, 1994; Bartolini, 2003). Also, the presence of steryl ethers in the Pacific which may be biomarkers of cool water, high seasonal productivity and/or nutrient input by upwelling (Brassell, 2009). A significant nutrient input from upwelling on the central Moroccan margin should enhance an oceanic crust signature in the sediments and it should be more pronounced in the distal setting (Hole 416A) which is closer to possible oceanic upwelling.

Is there any geochemical change on the central Moroccan margin during the Weissert Event?

In the proximal Zalidou section, the steady stratigraphic trends in the selected major element contents (Al_2O_3, SiO_2 and CaO) support that continental weathering and the input of detrital material, from both coarse- and fine-grained minerals, was stable throughout the Valanginian stage (Fig. 4). The trace elements associated with detrital and continental sources (e.g., Li and Nd) also display a steady trend (Fig. 4), supporting an almost continuous weathering and hydrolysis regime. However, the consistently low concentrations of HFSE (i.e., Zr and Hf) in

the upper part of the Weissert Event (between 25.05 and 32.8 m, *O. nicklesi* ammonite Subzone, NK3B and CC4a nannofossil subzones; see Fig. 4 and Supplementary Table) suggest low deposition of coarse-grained clastics (i.e., quartz). This may be related to the sandy-marlstones (fine-grained lithology) of this interval, which were deposited under conditions of sea-level rise (maximal flooding; Reboulet et al., 2022). The calculated CIA is generally steady, further supporting a constant rate of hydrolysis on the continent. The slightly higher values at the same level where HFSE have low concentrations might reflect higher contents of fine-grained material, such as alluminosilicates, related to the deeper depositional setting. Furthermore, the unchanged Pb, Sr and Nd isotopic ratios do not support any geochemical change during the Valanginian stage (Fig. 6).

In the distal Hole 416A, the stable SiO_2 content and CIA suggest, respectively, a steady input of coarse-grained clastic material and a constant rate of hydrolysis for the entire Valanginian stage (Fig. 4). However, the increasing Al_2O_3 content suggests higher input of fine-grained detrital material within the Weissert Event (from 1280.71 to 1187.94 mbsf, upper NK3A to NK3B and upper CC3b to CC4a nannofossil subzones). A concomitant reduction in carbonate deposition is also suggested from the decreasing CaO content. Such changes are evident at the beginning of the Weissert Event within the lithological unit VI. In the lower part of that unit, two calcareous and quartz-rich turbidite cycles are recognized, whereas, in its upper part, the cycles are uniform and grade from sandstone to marlstone and claystone (Lancelot et al., 1980). The level of this lithological change is not certain, occurring gradually, and was first recorded at ~1299 mbsf (core 22). Additionally, the increase in Li concentration during the Weissert Event (upper NK3A to NK3B, and upper CC3b to CC4a nannofossil subzones) complements the observation from major elements (Fig. 4) since the proportion of clays controls lithium contents. The input of continental and coarse-grained clastics was probably steady, as observed from the uniform HFSE and REE contents (Fig. 4; Supplementary Table).

Finally, the Pb, Sr and Nd isotopic ratios do not show any significant change throughout the studied Valanginian interval (Fig. 6); even if inter-sample variations in Sr and Nd are observed, they are most probably related to the increase in clay-mineral deposition during the Weissert Event.

In summary, there is no significant change in the sediment major and trace element concentrations on the central Moroccan margin during the Valanginian stage. The few stratigraphic variations in major and trace element concentrations are most probably caused by variations in sediment lithology, with higher clay input and lower detrital quartz input during the upper part of the Weissert Event in Zalidou and within the identified Weissert Event interval in Hole 416A. Similarly, the radiogenic isotopes Pb, Sr and Nd do not show any significant trend during the Valanginian stage, suggesting no major change in the source material during the Event.

How do sediments from proximal and distal sites compare?

The distal Hole 416A shows a simple binary mixture of clay and carbonate sediment. In contrast, the proximal Zalidou section shows a more complicated mixture of detrital deposits with a continental origin (silica-rich and clay) and carbonates. This complexity is depicted by the distribution of the major elements (Fig. 3). Hole 416A sediments are relatively rich in Al-rich components such as fine-grained clays (i.e., aluminosilicates). The Zalidou sediments are relatively rich in coarse-grained Si-rich components (i.e., quartz), as shown by the slightly higher SiO_2 content. It is noteworthy that the analyzed samples correspond to fine-grained lithologies, as was avoided the sampling of coarse-grained sediment. The observed difference between sites (proximal *versus* distal) is caused by the different depositional settings. Clays are light-weight minerals and can travel further and accumulate in the deeper setting (Hole 416A). In contrast, coarse-grained clastic minerals are heavy and accumulate in the proximal setting close to river output (Zalidou).

Differences in the concentrations of trace elements between Zalidou and Hole 416A also highlight their different depositional settings. The higher concentrations of Li in Hole 416A reflect the more significant proportion of clays compared with Zalidou (Fig. 5a), since Li is concentrated in fine-grained minerals rather than coarse-grained minerals (Sauzéat et al., 2015; and references therein). Additionally, Li could reflect a higher proportion of authigenic clay minerals in Hole 416A rather than detrital clays (see Andrews et al., 2020; and references therein). The concentration of Nd is marginally higher in Hole 416A compared with Zalidou, indicating that both successions record input from continental detrital material. Lastly, the high Zr concentration in Zalidou compared to Hole 416A (Fig. 5d), is explained by its proximal depositional setting close to the fluvial input of coarse clastic minerals. Zirconium, like other HFSE reside in heavy minerals such as zircon, minerals that are not transported far in a basin and are deposited close to the continental margin (Patchett et al., 1984). In contrast, fine-grained clays (light-weight) deposited farther away from the continent show deficiencies in Zr and Hf.

The initial isotope ratios of Pb, Sr and Nd are comparable between both studied successions except for few differences. The slightly more radiogenic $^{208}Pb/^{204}Pb_{(i)}$ and $^{87}Sr/^{86}Sr_{(i)}$ ratios in Hole 416A compared to Zalidou can be explained by a contribution from a source of more radiogenic sediments (Figs. 7b and 7c). In summary, the geochemical differences observed between the two studied successions relate mainly to their depositional setting (proximal *versus* distal) and to the associated chemical fractionation occurring during the transport of sediments.

Is there volcanic input during the Weissert Event?

The aforementioned environmental perturbations are tentatively linked to extensive volcanism from the Paraná-Etendeka large igneous province (LIP) of South America – SW Africa (Weissert et al., 1998; Erba et al., 2004) or the Comei-Bunbury LIP of SE Tibet – SW

Australia (Zhu et al., 2009). Uncertainties related to age models (e.g., scarcity of data, uncertainty in age models and in absolute age calibration) hinder direct temporal correlation between these LIPs and the Weissert Event (Charbonnier et al., 2017). Radiometric ages of basalts from the Paraná-Etendeka LIP (135.5–126 Ma; e.g., Thompson et al., 2001; Trumbull et al., 2004; Almeida et al., 2018; Baksi, 2018; Rocha et al., 2020; Bacha et al., 2021) and the Comei-Bunbury LIP (134–123 Ma; e.g., Zhu et al., 2008, 2009; Liu et al., 2015) likely post-date the onset of the Valanginian positive carbon-isotope excursion (135.22 ±1.0 Ma; Martinez et al., 2015). Moreover, Charbonnier et al. (2017) observed mercury enrichments interpreted as volcanic in origin in sediments at or near the onset of the Weissert Event from the Central Tethys. Fesneau et al. (2009) observed an ochre-colored layer of lower Valanginian age in the Vocontian Basin (France) enriched in trace elements with a specific magmatic affinity (Zr, Ba, Th, Y, Hf, U, Pb, Nb, Ta). The layer was interpreted as "bentonite" of volcanic origin. These studies cannot designate unambiguously if one or both LIPs were involved during the Weissert Event. Chavagnac et al. (2008) and Peate (2009) observed overlapping Pb isotopic compositions from Hole 1149B and magmas from the Paraná-Etendeka LIP. The majority of samples which show a Pb isotopic shift in Hole 1149B (upper lithological unit IV; Core 20R to 16R) belong to the Hauterivian stage (Lozar and Tremolada, 2003), and the Nd-Sr isotope ratios were not compared with the aforementioned LIPs. Using a combination of Pb, Sr and Nd isotopes should constrain the relationship between any of the aforementioned LIPs and the Weissert Event. For example, a volcanic contribution to the sediments is expected to cause a more radiogenic Nd isotopic composition (i.e., radiogenic mantle source) and less radiogenic Sr and Pb isotope ratios.

On the central Moroccan margin, the Nd isotopic composition in both studied successions does not increase to more radiogenic ratios (Fig. 6). Furthermore, Figure 8 compares the initial isotope ratios (135 Ma) of Pb, Sr and Nd obtained on the central Moroccan margin

sediments to those published for the suggested Valanginian LIPs. Lead and Sr isotopic ratios of the sediments overlap with the higher ratios reported for the Paraná-Etendeka LIP, at $^{206}Pb/^{204}Pb_{(i)}$ >18.5, $^{207}Pb/^{204}Pb_{(i)}$ >15.66, $^{208}Pb/^{204}Pb_{(i)}$ >38.5 and $^{87}Sr/^{86}Sr_{(i)}$ > 0.708. However, the Nd isotopic ratios are lower on the central Moroccan margin sediments ($^{143}Nd/^{144}Nd_{(i)}$< 0.5120) to any of the LIPs ($^{143}Nd/^{144}Nd_{(i)}$> 0.5120) shown in Figure 8d. This difference is a strong argument against a significant role of volcanic material from the LIPs to sediment during the Valanginian stage on the central Moroccan margin.

Continental runoff versus upwelling as causing eutrophication

The trace element patterns of Zalidou and Hole 416A normalized to the upper continental crust (UCC) values of Rudnick and Gao (2013) are shown in Figure S3. The studied successions show trace elements patterns similar to the UCC for the majority of elements. This similarity suggests that the sediment trace-element budget is controlled by material with a continental origin. The few element enrichments/depletions relative to the UCC are caused by the chemical fractionation of elements occurring during sediment transport (see caption Fig. S3). As a consequence, the trace element patterns of Hole 416A bulk sediments exclude the possibility of a significant role of nutrient input from oceanic upwelling to the composition of the deposits. The Hole 416A sediments have a chemical signature primarily controlled by terrigenous input. Indeed, the sedimentation rate in Hole 416A is high (65 m Myr^{-1}) and the sediments are dominated by detrital material (Lancelot et al., 1980). Also, Carpentier et al. (2013) demonstrated that offshore settings close to continental shelves have a chemical composition (signature) similar to the nearby continental source areas. Alternatively, during the Valanginian the oceanic and atmospheric conditions were not severe such that they did not induce significant upwelling on this part of the Moroccan margin.

Our new isotope results also support that upwelling did not significantly contribute to Hole 416A sediments. In principle, strong upwelling should induce a “juvenile” oceanic crust

isotopic signature to the sediments. However, this is not the case at Hole 416A. First, the Pb and Sr isotopic ratios of Hole 416A sediments are very similar to those of the Zalidou proximal sediments, supporting the interpretation that they were fed by the same continental source (Fig. 7). Second, the average ε_{Nd} values in the two studied successions are identical (~ –12 ±1; Supplementary Table) and of continental origin, even lower than the average upper continental crust value (−10.3 ± 1.2, 1σ) reported by Chauvel et al. (2014). These similar values further support a common continental source for Zalidou and Hole 416A and undermine a significant contribution to the sediments from upwelling.

What is the source of the central Moroccan margin sediments?

The Pb, Sr and Nd isotopic compositions of the central Moroccan margin sediments are dominated by continental material. Therefore, it is worth comparing the isotopic composition of sediments to what is known for the surrounding crustal areas exposed during the Valanginian in order to establish the source area(s). Lead and Nd isotopes are particularly useful in this respect because model ages can be calculated for both isotopic systems. Such model ages do not provide a precise measure of the age of the eroded material. Still, they estimate the average age of formation of the material eroded from the continental crust. The slope defined by the central Moroccan margin sediments in a $^{206}Pb/^{204}Pb_{(m)}$ *versus* $^{207}Pb/^{204}Pb_{(m)}$ isotopic space (Fig. S4 and its caption) provides an average model age of about 1.1 Ga for the source of the sediments. In comparison, Nd isotopes provide a model age of about 1.9 Ga when using the parameters from Chauvel et al. (2008 and 2014). Therefore, both isotopic systems suggest that the central Moroccan margin was fed by sediments from an old and continental “cratonic” source. Additionally, the source of sediments did not change during the Valanginian stage, as observed from the unchanged isotopic ratios of Pb, Sr and Nd (Fig. 6).

The best approach to trace the origin of sediments deposited in the basin is to compare the isotopic compositions of sediments and potential sources in the area. We measured Pb, Sr and Nd isotopes in the sediments but studies of potential sources reporting data for the combined three isotopic systems are limited. Thereby, we considered only Nd and Sr isotopes in Figure 9 because they are the only two isotopic systems for which an extensive database exists. Because most published data on the potential sources do not report the parent-daughter isotope ratios, we calculated their initial isotope ratios at 135 Ma (Supplementary Table) using the recommended Sm/Nd and Rb/Sr ratios for the upper continental crust (Rudnick and Gao, 2013).

Given that these terranes are old crustal materials, it should not be a problem.

In the Sr-Nd space of Figure 9, the central Moroccan margin sediments overlap with the African dust sources (Sahara region; Fig. S5), both having $^{143}Nd/^{144}Nd_{(m)}$ ratios clustering between 0.5118 – 0.5120. The Sr isotopic composition of the African dust sources is highly variable and generally more radiogenic than that of the central Moroccan margin sediments (Fig. 9), but it is probably due to the fine size of dust particles naturally more concentrated in Rb-rich clays and consequently have more radiogenic Sr isotope ratios. Moreover, the studied sediments lie in between two additional end-members: (1) the West African Craton (2.1 Ga) (Fig. S5); and (2) the surrounding Moroccan massifs as the NE Meseta (344 Ma), Anti-Atlas (560–543 Ma) and the central Jebilet (240 Ma) (Fig. 9 and Fig. S5). The contribution of sediments *via* fluvial input from both of these "cratonic" end-members is highly plausible considering their geographic proximity to the studied successions. It is noteworthy that the Jebilet massif and the Anti-Atlas are closer to the Zalidou section (see Fig. 1a and Fig. S5), whereas the Moroccan Meseta is closer to the Hole 416A (Fig. S5).

The slightly more radiogenic Pb and Sr ratios observed in Hole 416A compared with Zalidou (Figs. 7b and 7c) might have their origin in a relatively less important contribution of fluvial-

input in the offshore succession, resulting in a more significant signature of the dust component. Figure S6 compares the initial Pb and Sr isotope ratios of sediments in Zalidou and Hole 416A with surrounding areas for which data exist for these isotopic systems; it suggests that the far African Sahara regions (Saharan metacraton and Sahel Desert; Fig. S5) could cause such a shift to more radiogenic Pb and Sr isotopic ratios. Nonetheless, surface winds blew SW over north Africa during the Cretaceous (Poulsen et al., 1998), so the relatively northward Hole 416A should hypothetically receive less dust input (see Fig. 1a and Fig. S5). Accordingly, fluvial input from other massifs more proximal to Hole 416A (e.g., the middle Atlas) could have caused this difference, but we can not test for their contribution due to the lack of isotope studies.

In summary, the isotopic signature of the central Moroccan margin sediments is dominated by old continental sources. The African Sahara regions could have significantly contributed to the central Moroccan margin sediments through wind transport. Today, the Sahara and north African terrains are known as the most important dust sources to the Atlantic Ocean (e.g., Grousset and Biscaye, 2005; Abouchami et al., 2013). During the Valanginian stage (137.7–132.6 Ma), dust input from old African terrains located eastward could be similarly expected. Indeed, the wind circulation models of Price et al. (1995) demonstrate west and SW wind vectors over north Africa in the Jurassic and the Cretaceous. Additionally, the surrounding Moroccan massifs could have contributed to the sediments *via* direct fluvial transport.

Conclusions

Valanginian carbonate deposits from two geological successions on the central Moroccan margin show geochemical signatures characteristic of their respective depositional settings (proximal *versus* distal). The onshore Zalidou section consists of a mixture of detrital (silica-rich and clay) and carbonate materials, while the offshore DSDP Hole 416A shows a binary mixture of clay and carbonate. The major and trace elements show higher coarse-detrital input

(silica-rich) in the Zalidou section and higher authigenic clay input (aluminosilicates) in Hole 416A. This is due to mineral sorting processes occurring during the transport of sediments, leading to the chemical fractionation of some elements. Nonetheless, the similar radiogenic isotope signature between both sites suggests a common “old” and continental source for all sediments. No trace of a significant input from oceanic upwelling can be detected in the distal site sediments. This suggests that the central Moroccan margin was primarily fed by nutrients from continental runoff and weathering before, during and after the Weissert Event. The source of sediments also did not change throughout the studied Valanginian interval and was most probably the African Sahara regions.

No volcanic contribution from the Paraná-Etendeka or the Comei-Bunbury large igneous provinces (LIPs) were detected in the sediments during the entire Valanginian stage. If any such material reached the central Moroccan margin, the quantities must have been small enough to not modify the dominantly continental signature of the sediments. It can not be excluded that volcanic material might have affected seawater without changing the composition of deposited sediments during the Weissert Event. It is therefore difficult to imagine that the LIPs triggered the Weissert Event recorded in the studied area. Our study shows the potential of combining several radiogenic isotopes to test for a volcanic contribution in sediments during the Weissert Event, and to identify the specific LIP that was involved.

Acknowledgements:

Pamela Gutiérrez, Pascale Louvat and Pierre Burckel are warmly thanked for their help in the chemistry lab and for their assistance during the MC-ICP-MS and ICP-MS measurements. This work benefited of financial support from the Ministries of foreign affairs from France and Morocco (PHC project n° 031/STU/13), the French IRD, Campus France and various grants from ISTerre, the Laboratoire de Géologie de Lyon, the OSUG@2020

Labex, the CNRS SYSTER program and IODP France soutien post-cruise. We are grateful to the editor Dr. Kirsty Marie Edgar and two anonymous reviewers for their journal pre-proof corrections and comments which greatly improved the quality of an earlier version of the manuscript.

References

1. Abouchami, W., Näthe, K., Kumar, A., Galer, S.J.G., Jochum, K.P., Williams, E., Horbe, A.M.C., Rosa, J.W.C., Balsam, W., Adams, D., Mezger, K., Andreae, M.O., 2013. Geochemical and isotopic characterization of the bodélé depression dust source and implications for transatlantic dust transport to the Amazon basin. Earth Planet. Sci. Lett. 380, 112–123. https://doi.org/10.1016/j.epsl.2013.08.028
2. Allen, C.M., Wooden, J.L. and Chappell, B.W., 1997. Late Paleozoic crustal history of central coastal Queensland interpreted from geochemistry of Mesozoic plutons: The effects of continental rifting. Lithos, 42(1-2), 67-88. https://doi.org/10.1016/S0024-4937(97)00037-6
3. Aguado, R., Company, M., Castro, J.M., de Gea, G.A., Molina, J.M., Nieto, L.M., Ruiz-Ortiz, P.A., 2018. A new record of the Weissert episode from the Valanginian succession of Cehegín (Subbetic, SE Spain): Bio- and carbon isotope stratigraphy. Cretac. Res. 92, 122–137. https://doi.org/10.1016/j.cretres.2018.07.010
4. Aguirre-Urreta, M.B., Price, G.D., Ruffell, A.H., Lazo, D.G., Kalin, R.M., Ogle, N., Rawson, P.F., 2008. Southern Hemisphere Early Cretaceous (Valanginian-Early Barremian) carbon and oxygen isotope curves from the Neuquén Basin, Argentina. Cretac. Res. 29, 87–99. https://doi.org/10.1016/j.cretres.2007.04.002
5. Ajaji, T., Weis, D., Giret, A., Bouabdellah, M., 1998. Coeval potassic and sodic calc-alkaline series in the post-collisional Hercynian Tanncherfi intrusive complex, northeastern Morocco: Geochemical, isotopic and geochronological evidence. Lithos

45, 371–393. https://doi.org/10.1016/S0024-4937(98)00040-1

6. Almeida, V. V., Janasi, V.A., Heaman, L.M., Shaulis, B.J., Hollanda, M.H.B.M., Renne, P.R., 2018. Contemporaneous alkaline and tholeiitic magmatism in the Ponta Grossa Arch, Paraná-Etendeka Magmatic Province: Constraints from U–Pb zircon/baddeleyite and 40Ar/39Ar phlogopite dating of the José Fernandes Gabbro and mafic dykes. J. Volcanol. Geotherm. Res. 355. https://doi.org/10.1016/j.jvolgeores.2017.01.018
7. Andrews, E., Pogge von Strandmann, P.A.E., Fantle, M.S., 2020. Exploring the importance of authigenic clay formation in the global Li cycle. Geochim. Cosmochim. Acta 289, 47–68. https://doi.org/10.1016/j.gca.2020.08.018
8. Arthur, M.A., Brumsack, H.J., Jenkyns, H.C., Schlanger, S.O., 1990. Stratigraphy, geochemistry, and paleoceanography of organic carbon- rich Cretaceous sequences. Cretac. Resour. events Rhythm. https://doi.org/10.1007/978-94-015-6861-6_6
9. Bacha, R.R., Waichel, B.L. and Ernst, R.E., 2022. The mafic volcanic climax of the Paraná-Etendeka Large Igneous Province as the trigger of the Weissert Event. Terra Nov. 34(1), 28-36. https://doi.org/10.1111/ter.12558
10. Baksi, A.K., 2018. Paraná flood basalt volcanism primarily limited to ~ 1 Myr beginning at 135 Ma: New 40Ar/39Ar ages for rocks from Rio Grande do Sul, and critical evaluation of published radiometric data. J. Volcanol. Geotherm. Res. 355. https://doi.org/10.1016/j.jvolgeores.2017.02.016
11. Barreto, C.J.S., Lafon, J.M., De Lima, E.F., Sommer, C.A., 2016. Geochemical and Sr-Nd-Pb isotopic insight into the low-Ti basalts from southern Paraná Igneous Province, Brazil: The role of crustal contamination. Int. Geol. Rev. 58, 1324–1349. https://doi.org/10.1080/00206814.2016.1147988
12. Bartolini, A., 2003. Cretaceous radiolarian biochronology and carbon isotope

stratigraphy of ODP Site 1149 (northwestern Pacific, Nadezhda Basin). Proc. Ocean Drill. Progr. Sci. Results 185. https://doi.org/10.2973/odp.proc.sr.185.011.2003

13. Bea, F., Montero, P., Haissen, F., El Archi, A., 2013. 2.46Ga kalsilite and nepheline syenites from the Awsard pluton, Reguibat Rise of the West African Craton, Morocco. Generation of extremely K-rich magmas at the Archean-Proterozoic transition. Precambrian Res. 224, 242–254. https://doi.org/10.1016/j.precamres.2012.09.024
14. Belkacim, S., Gasquet, D., Liégeois, J.P., Arai, S., Gahlan, H.A., Ahmed, H., Ishida, Y., Ikenne, M., 2017. The Ediacaran volcanic rocks and associated mafic dykes of the Ouarzazate Group (Anti-Atlas, Morocco): Clinopyroxene composition, whole-rock geochemistry and Sr-Nd isotopes constraints from the Ouzellarh-Siroua salient (Tifnoute valley). J. African Earth Sci. 127, 113–135. https://doi.org/10.1016/j.jafrearsci.2016.08.002
15. Bersezio, R., Erba, E., Gorza, M., Riva, A., 2002. Berriasian-Aptian black shales of the Maiolica formation (Lombardian Basin, Southern Alps, Northern Italy): Local to global events. Palaeogeogr. Palaeoclimatol. Palaeoecol. 180, 253–275. https://doi.org/10.1016/S0031-0182(01)00416-3
16. Blanc, A., Bernard-Griffiths, J., Caby, R., Caruba, C., Caruba, R., Dars, R., Fourcade, S., Peucat, J.J., 1992. U-Pb dating and isotopic signature of the alkaline ring complexes of Bou Naga (Mauritania): its bearing on late proterozoic plate tectonics around the West African craton. J. African Earth Sci. 14, 301–311. https://doi.org/10.1016/0899-5362(92)90034-A
17. Boher, M., Abouchami, W., Michard, A., Albarede, F., Arndt, N.T., 1992. Crustal growth in West Africa at 2.1 Ga. J. Geophys. Res. 97, 345–369. https://doi.org/10.1029/91JB01640
18. Bomou, B., Adatte, T., Tantawy, A. A., Mort, H., Fleitmann, D., Huang, Y., & Föllmi,

K. B., 2013. The expression of the Cenomanian–Turonian oceanic anoxic event in Tibet. Palaeogeogr. Palaeoclimatol. Palaeoecol. 369, 466–481. https://doi.org/10.1016/j.palaeo.2012.11.011

19. Bornemann, A., Mutterlose, J., 2008. Calcareous Nannofossil and ^{13}C Records from the Early Cretaceous of the Western Atlantic Ocean: Evidence for Enhanced Fertilization across the Berriasian-Valanginian Transition. Palaios 23, 821–832. https://doi.org/10.2110/palo.2007.p07-076r
20. Bouloton, J., Gasquet, D., Pin, C., 2019. Petrogenesis of the Early-Triassic quartz-monzodiorite dykes from Central Jebilet (Moroccan Meseta): Trace element and Nd-Sr isotope constraints on magma sources, and inferences on their geodynamic context. J. African Earth Sci. 149, 451–464. https://doi.org/10.1016/j.jafrearsci.2018.08.023
21. Brassell, S.C., 2009. Steryl ethers in a Valanginian claystone: Molecular evidence for cooler waters in the central Pacific during the Early Cretaceous? Palaeogeogr. Palaeoclimatol. Palaeoecol. 282, 45–57. https://doi.org/10.1016/j.palaeo.2009.08.009
22. Carignan, J., Hild, P., Mevelle, G., Morel, J., Yeghicheyan, D., 2001. Routine analyses of trace elements in geological samples using flow injection and low pressure on-line liquid chromatography coupled to ICP-MS: A study of geochemical reference materials BR, DR-N, UB-N, AN-G and GH. Geostand. Newsl. 25, 187–198. https://doi.org/10.1111/j.1751-908x.2001.tb00595.x
23. Carpentier, M., Chauvel, C., Maury, R.C., Mattielli, N., 2009. The “zircon effect” as recorded by the chemical and Hf isotopic compositions of Lesser Antilles forearc sediments. Earth Planet. Sci. Lett. 287, 86–99. https://doi.org/10.1016/j.epsl.2009.07.043
24. Carpentier, M., Weis, D., Chauvel, C., 2013. Large U loss during weathering of upper continental crust: The sedimentary record. Chem. Geol. 340, 91–104.

https://doi.org/10.1016/j.chemgeo.2012.12.016

25. Čepek, P., Gartner, S., 1980. Mesozoic Calcareous Nannofossils, Deep Sea Drilling Project sites 415 and 416, Moroccan Basin 345–351. https://doi.org/10.2973/dsdp.proc.50.108.1980
26. Chalot-Prat, F., 1995. Genesis of rhyolitic ignimbrites and lavas from distinct sources at a deep crustal level: field, petrographie, chemical and isotopic (Sr, Nd) constraints in the Tazekka volcanic complex (Eastern Morocco). Lithos 36, 29–49. https://doi.org/10.1016/0024-4937(95)00004-Y
27. Channell, J.E.T., Erba, E., Lini, A., 1993. Magnetostratigraphic calibration of the Late Valanginian carbon isotope event in pelagic limestones from Northern Italy and Switzerland. Earth Planet. Sci. Lett. 118, 145–166. https://doi.org/10.1016/0012-821X(93)90165-6
28. Charbonnier, G., Boulila, S., Gardin, S., Duchamp-Alphonse, S., Adatte, T., Spangenberg, J.E., Föllmi, K.B., Colin, C., Galbrun, B., 2013. Astronomical calibration of the Valanginian "Weissert" episode: The Orpierre marl-limestone succession (Vocontian Basin, southeastern France). Cretac. Res. 45, 25–42. https://doi.org/10.1016/j.cretres.2013.07.003
29. Charbonnier, G., Morales, C., Duchamp-Alphonse, S., Westermann, S., Adatte, T., Föllmi, K.B., 2017. Mercury enrichment indicates volcanic triggering of Valanginian environmental change. Sci. Rep. 7. https://doi.org/10.1038/srep40808
30. Charbonnier, G., Duchamp-Alphonse, S., Deconinck, J.F., Adatte, T., Spangenberg, J.E., Colin, C., Föllmi, K.B., 2020. A global palaeoclimatic reconstruction for the Valanginian based on clay mineralogical and geochemical data. Earth-Science Rev. 202, 103092. https://doi.org/10.1016/j.earscirev.2020.103092
31. Chauvel, C., Lewin, E., Carpentier, M., Arndt, N.T., Marini, J.C., 2008. Role of

recycled oceanic basalt and sediment in generating the Hf-Nd mantle array. Nat. Geosci. 1. https://doi.org/10.1038/ngeo.2007.51

32. Chauvel, C., Bureau, S., Poggi, C., 2011. Comprehensive Chemical and Isotopic Analyses of Basalt and Sediment Reference Materials. Geostand. Geoanalytical Res. 35, 125–143. https://doi.org/10.1111/j.1751-908X.2010.00086.x
33. Chauvel, C., Garçon, M., Bureau, S., Besnault, A., Jahn, B. ming, Ding, Z., 2014. Constraints from loess on the Hf-Nd isotopic composition of the upper continental crust. Earth Planet. Sci. Lett. 388, 48–58. https://doi.org/10.1016/j.epsl.2013.11.045
34. Chavagnac, V., German, C.R., Taylor, R.N., 2008. Global environmental effects of large volcanic eruptions on ocean chemistry: Evidence from "hydrothermal" sediments (ODP Leg 185, Site 1149B). J. Geophys. Res. Solid Earth 113, 1–17. https://doi.org/10.1029/2007JB005333
35. Direen, N.G., Cohen, B.E., Maas, R., Frey, F.A., Whittaker, J.M., Coffin, M.F., Meffre, S., Halpin, J.A. and Crawford, A.J., 2017. Naturaliste Plateau: constraints on the timing and evolution of the Kerguelen Large Igneous Province and its role in Gondwana breakup. Australian Journal of Earth Sciences, 64(7), 851-869. https://doi.org/10.1080/08120099.2017.1367326
36. Duchamp-Alphonse, S., Gardin, S., Fiet, N., Bartolini, A., Blamart, D., Pagel, M., 2007. Fertilization of the northwestern Tethys (Vocontian basin, SE France) during the Valanginian carbon isotope perturbation: Evidence from calcareous nannofossils and trace element data. Palaeogeogr. Palaeoclimatol. Palaeoecol. 243, 132–151. https://doi.org/10.1016/j.palaeo.2006.07.010
37. EL Haibi, H., EL Hadi, H., Tahiri, A., Martínez Poyatos, D., Gasquet, D., Pérez-Cáceres, I., González Lodeiro, F., Mehdioui, S., 2020. Geochronology and isotopic geochemistry of Ediacaran high-K calc-alkaline felsic volcanism: An example of a

Moroccan perigondwanan (Avalonian?) remnant in the El Jadida horst (Mazagonia). J. African Earth Sci. 163, 103669. https://doi.org/10.1016/j.jafrearsci.2019.103669

38. Ellouz, N., Patriat, M., Gaulier, J.M., Bouatmani, R., Sabounji, S., 2003. From rifting to Alpine inversion: Mesooic and Cenozoic subsidence history of some Moroccan basins. Sediment. Geol. 156, 185–212. https://doi.org/10.1016/S0037-0738(02)00288-9
39. Erba, E., Bartolini, A., Larson, R.L., 2004. Valanginian Weissert oceanic anoxic event. Geology 32, 149–152. https://doi.org/10.1130/G20008.1
40. Erba, E., Tremolada, F., 2004. Nannofossil carbonate fluxes during the Early Cretaceous: Phytoplankton response to nutrification episodes, atmospheric CO_2, and anoxia. Paleoceanography 19, n/a-n/a. https://doi.org/10.1029/2003PA000884
41. Essaifi, A., Samson, S., Goodenough, K., 2014. Geochemical and Sr-Nd isotopic constraints on the petrogenesis and geodynamic significance of the Jebilet magmatism (Variscan Belt, Morocco). Geol. Mag. 151, 666–691. https://doi.org/10.1017/S0016756813000654
42. Essaifi, A., Zayane, R., 2018. Petrogenesis and origin of the Upper Jurassic-Lower Cretaceous magmatism in Central High Atlas (Morocco): Major, trace element and isotopic (Sr-Nd) constraints. J. African Earth Sci. 137, 229–245. https://doi.org/10.1016/j.jafrearsci.2017.10.002
43. Ewart, A., Schon, R.W. and Chappell, B.W., 1992. The Cretaceous volcanic-plutonic province of the central Queensland (Australia) coast—a rift related 'calc-alkaline'province. Earth and Environmental Science Transactions of the Royal Society of Edinburgh, 83(1-2), 327-345. https://doi.org/10.1017/S0263593300008002
44. Ewart, A., Milner, S.C., Armstrong, R.A., Duncan, A.R., 1998a. Etendeka Volcanism of the Goboboseb Mountains and Messum Igneous Complex, Namibia. Part I:

Geochemical Evidence of Early Cretaceous Tristan Plume Melts and the Role of Crustal Contamination in the Parana´–Etendeka CFB. J. Petrol. 39, 227–253. https://doi.org/10.1093/petroj/39.2.227

45. Ewart, A., Milner, S.C., Armstrong, R.A., Duncan, A.R., 1998b. Etendeka volcanism of the Goboboseb Mountains and Messum Igneous Complex, Namibia. Part I: Geochemical evidence of early cretaceous Tristan plume melts and the role of crustal contamination in the Paraná-Etendeka CFB. J. Petrol. 39, 191–225. https://doi.org/10.1093/petroj/39.2.191
46. Ewart, A., Marsh, J.S., Milner, S.C., Duncan, A.R., Kamber, B.S., Armstrong, R.A., 2004a. Petrology and geochemistry of early cretaceous bimodal continental flood volcanism of the NW Etendeka, Namibia. part 2: Characteristics and petrogenesis of the high-Ti Latite and high-Ti and low-Ti voluminous quartz Latite Eruptives. J. Petrol. 45, 107–138. https://doi.org/10.1093/petrology/egg082
47. Ewart, A., Marsh, J.S., Milner, S.C., Duncan, A.R., Kamber, B.S., Armstrong, R.A., 2004b. Petrology and geochemistry of early cretaceous bimodal continental flood volcanism of the NW Etendeka, Namibia. part 1: Introduction, mafic lavas and re-evaluation of mantle source components. J. Petrol. 45, 59–105. https://doi.org/10.1093/petrology/egg083
48. Faure, G., 1986. Principles of isotope geology. Second edition. John Wiley Sons.
49. Fesneau, C., Deconinck, J.F., Pellenard, P., Reboulet, S., 2009. Evidence of aerial volcanic activity during the Valanginian along the northern Tethys margin. Cretac. Res. 30, 533– 539. https://doi.org/10.1016/j.cretres.2008.09.004
50. Föllmi, K.B., Weissert, H., Bisping, M., Funk, H., 1994. Phosphogenesis, carbon-isotope stratigraphy, and carbonate-platform evolution along the Lower Cretaceous northern Tethyan margin. Geol. Soc. Am. Bull. 106, 729–746.

https://doi.org/10.1130/0016-7606(1994)106<0729:PCISAC>2.3.CO;2

51. Föllmi, K.B., Godet, A., Bodin, S., Linder, P., 2006. Interactions between environmental change and shallow water carbonate buildup along the northern Tethyan margin and their impact on the Early Cretaceous carbon isotope record. Paleoceanography 21, 1–16. https://doi.org/10.1029/2006PA001313
52. Föllmi, K.B., 2012. Early Cretaceous life, climate and anoxia. Cretac. Res. 35, 230–257. https://doi.org/10.1016/j.cretres.2011.12.005
53. Frey, F.A., McNaughton, N.J., Nelson, D.R., DeLaeter, J.R., Duncan, R.A., 1996. Petrogenesis of the Bunbury Basalt, Western Australia: Interaction between the Kerguelen plume and Gondwana lithosphere Earth Planet. Sci. Lett. 144, 163–183. https://doi.org/10.1016/0012-821x(96)00150-1
54. Frizon de Lamotte, D., Zizi, M., Missenard, Y., Hafid, M., El Azzouzi, M., Maury, R.C., Charrière, A., Taki, Z., Benammi, M., Michard, A., 2008. The Atlas system. Lect. Notes Earth Sci. 116, 133–202. https://doi.org/10.1007/978-3-540-77076-3_4
55. Frizon de Lamotte, D., Leturmy, P., Missenard, Y., Khomsi, S., Ruiz, G., Saddiqi, O., Guillocheau, F., Michard, A., 2009. Mesozoic and Cenozoic vertical movements in the Atlas system (Algeria, Morocco, Tunisia): An overview. Tectonophysics 475, 9–28. https://doi.org/10.1016/j.tecto.2008.10.024
56. Gasquet, D., Leterrier, J., Mrini, Z., Vidal, P., 1992. Petrogenesis of the Hercynian Tichka plutonic complex (Western High Atlas, Morocco): Trace element and RbSr and SmNd isotopic constraints. Earth Planet. Sci. Lett. 108, 29–44. https://doi.org/10.1016/0012-821X(92)90058-4
57. Gasquet, D., Levresse, G., Cheilletz, A., Azizi-Samir, M.R., Mouttaqi, A., 2005. Contribution to a geodynamic reconstruction of the Anti-Atlas (Morocco) during Pan-African times with the emphasis on inversion tectonics and metallogenic activity at the

Precambrian-Cambrian transition. Precambrian Res. 140, 157–182. https://doi.org/10.1016/j.precamres.2005.06.009

58. Gale, A. S., Mutterlose, J., Batenburg, S., Gradstein, F. M., Agterberg, F. P., Ogg, J. G., & Petrizzo, M. R., 2020. The Cretaceous Period. In Geologic Time Scale 2020. 1023-1086. Elsevier.
59. Gréselle, B., Pittet, B., Mattioli, E., Joachimski, M., Barbarin, N., Riquier, L., Reboulet, S., Pucéat, E., 2011. The Valanginian isotope event: A complex suite of palaeoenvironmental perturbations. Palaeogeogr. Palaeoclimatol. Palaeoecol. 306, 41–57. https://doi.org/10.1016/j.palaeo.2011.03.027
60. Gröcke, D.R., Price, G.D., Robinson, S.A., Baraboshkin, E.Y., Mutterlose, J., Ruffell, A.H., 2005. The Upper Valanginian (Early Cretaceous) positive carbon-isotope event recorded in terrestrial plants. Earth Planet. Sci. Lett. 240, 495–509. https://doi.org/10.1016/j.epsl.2005.09.001
61. Gross, A., Palchan, D., Krom, M.D., Angert, A., 2016. Elemental and isotopic composition of surface soils from key Saharan dust sources. Chem. Geol. 442, 54–61. https://doi.org/10.1016/j.chemgeo.2016.09.001
62. Grousset, F.E., Rognon, P., Coudé-Gaussen, G., Pédemay, P., 1992. Origins of peri-Saharan dust deposits traced by their Nd and Sr isotopic composition. Palaeogeogr. Palaeoclimatol. Palaeoecol. 93, 203–212. https://doi.org/10.1016/0031-0182(92)90097-O
63. Grousset, F.E., Parra, M., Bory, A., Martinez, P., Bertrand, P., Shimmield, G., Ellam, R.M., 1998. Saharan wind regimes traced by the Sr-Nd isotopic composition of subtropical Atlantic sediments: Last Glacial Maximum vs today. Quat. Sci. Rev. 17, 395–409. https://doi.org/10.1016/S0277-3791(97)00048-6
64. Grousset, F.E., Biscaye, P.E., 2005. Tracing dust sources and transport patterns using

Sr, Nd and Pb isotopes. Chem. Geol. 222, 149–167. https://doi.org/10.1016/j.chemgeo.2005.05.006

65. Hafid, M., Tari, G., Bouhadioui, D., Moussaid, I. El, Echarfaoui, H., Salem, A.A., Nahim, M., Dakki, M., 2008. Atlantic basins. Lect. Notes Earth Sci. 116, 303–329. https://doi.org/10.1007/978-3-540-77076-3_6
66. Hawkesworth, C.J., Mantovani, M.S.M., Taylor, P.N., Palacz, Z., 1986. Evidence from the Prana of south Brazil for a continental contribution to the Dupal basalts. Nature 322, 356–359.
67. Hennig, S., Weissert, H., Bulot, L., 1999. C-isotope stratigraphy, a calibration tool between ammonite- and magnetostratigraphy: The Valanginian-Hauterivian transition. Geol. Carpathica 50, 91–96.
68. Jaffey, A.H., Flynn, K.F., Glendenin, L.E., Bentley, W.C., Essling, A.M., 1971. Precision measurement of half-lives and specific activities of U235 and U238. Phys. Rev. C 4, 1889–1906. https://doi.org/10.1103/PhysRevC.4.1889
69. Jenkyns, H.C., 2003. Evidence for rapid climate change in the Mesozoic–Palaeogene greenhouse world. Philos. Trans. R. Soc. A Math. Phys. Eng. Sci. 361, 1885–1916. https://doi.org/10.1098/rsta.2003.1240
70. Jenkyns, H.C., 2010. Geochemistry of oceanic anoxic events. Geochemistry, Geophys. Geosystems 11, 1–30. https://doi.org/10.1029/2009GC002788
71. Jochum, K.P., Wilson, S.A., Abouchami, W., Amini, M., Chmeleff, J., Eisenhauer, A., Hegner, E., Iaccheri, L.M., Kieffer, B., Krause, J., Mcdonough, W.F., Mertz-Kraus, R., Raczek, I., Rudnick, R.L., Scholz, D., Steinhoefel, G., Stoll, B., Stracke, A., Tonarini, S., Weis, D., Weis, U., Woodhead, J.D., 2011. GSD-1G and MPI-DING Reference Glasses for In Situ and Bulk Isotopic Determination. Geostand. Geoanalytical Res. 35, 193–226. https://doi.org/10.1111/j.1751-908X.2010.00114.x

72. Jud, R., 1994. Biochronology and systematics of Early Cretaceous Radiolaria of the western Tethys.

73. Kuhn, O., Weissert, H., Föllmi, K.B., Hennig, S., 2005. Altered carbon cycling and trace-metal enrichment during the late Valanginian and early Hauterivian. Eclogae Geol. Helv. 98, 333–344. https://doi.org/10.1007/s00015-005-1172-7

74. Kujau, A., Heimhofer, U., Ostertag-Henning, C., Gréselle, B., Mutterlose, J., 2012. No evidence for anoxia during the Valanginian carbon isotope event-An organic-geochemical study from the Vocontian Basin, SE France. Glob. Planet. Change 92–93, 92–104. https://doi.org/10.1016/j.gloplacha.2012.04.007

75. Kujau, A., Heimhofer, U., Hochuli, P.A., Pauly, S., Morales, C., Adatte, T., Föllmi, K., Ploch, I., Mutterlose, J., 2013. Reconstructing Valanginian (Early Cretaceous) mid-latitude vegetation and climate dynamics based on spore-pollen assemblages. Rev. Palaeobot. Palynol. 197, 50–69. https://doi.org/10.1016/j.revpalbo.2013.05.003

76. Kumar, A., Abouchami, W., Galer, S.J.G., Garrison, V.H., Williams, E., Andreae, M.O., 2014. A radiogenic isotope tracer study of transatlantic dust transport from Africa to the Caribbean. Atmos. Environ. 82, 130–143. https://doi.org/10.1016/j.atmosenv.2013.10.021

77. Kump, L.R., Arthur, M.A., 1999. Interpreting carbon-isotope excursions: Carbonates and organic matter. Chem. Geol. 161, 181–198. https://doi.org/10.1016/S0009-2541(99)00086-8

78. Küster, D., Liégeois, J.P., Matukov, D., Sergeev, S., Lucassen, F., 2008. Zircon geochronology and Sr, Nd, Pb isotope geochemistry of granitoids from Bayuda Desert and Sabaloka (Sudan): Evidence for a Bayudian event (920-900 Ma) preceding the Pan-African orogenic cycle (860-590 Ma) at the eastern boundary of the Saharan Metacra. Precambrian Res. 164, 16–39.

https://doi.org/10.1016/j.precamres.2008.03.003

79. Lancelot, Y., Winterer, E.L., Bosellini, A., Boutefeu, G.A., Boyce, R.E., Cepek, P., Fritz, D., Galimov, E.M., Melguen, M., Price, I., Schlager, W., Sliter, W., Taguchi, K., Vincent, E., Westberg, J., 1980. Site 416, in the Moroccan Basin, Deep Sea Drilling Project Leg 50. Initial reports Deep Sea Drill. Proj. Leg 50, Funchal, Madeira Islands, 1976, 115–301. https://doi.org/10.2973/dsdp.proc.50.104.1980
80. Lozar, F., Tremolada, F., Ludden, J.N., Plank, T. and Escutia, C., 2003. Calcareous nannofossil biostratigraphy of Cretaceous sediments recovered at ODP Site 1149 (Leg 185, Nadezhda Basin, western Pacific). In Proc. Ocean Drill. Program Sci. Results, Vol. 185, 1-21
81. Le Roux, LJ, L. E. Glendenin, 1963. "Half-life of 232Th."Proceedings of the National Meeting on Nuclear Energy, Pretoria, South Africa. Vol. 83.
82. Le Roex, A.P., Lanyon, R., 1998. Isotope and trace element geochemistery of Cretaceous Damaraland lamprophyres and carbonatites, northwestern Namibia: evidence for plume-lithosphere interactions. J. Petrol. 39, 1117–1146. https://doi.org/10.1093/petroj/39.6.1117
83. Lini, A., Weissert, H., Erba, E., 1992. The Valanginian carbon isotope event: a first episode of greenhouse climate conditions during the Cretaceous. Terra Nov. 4, 374–384. https://doi.org/10.1111/j.1365-3121.1992.tb00826.x
84. Liu, Z., Zhou, Q., Lai, Y., Qing, C., Li, Y., Wu, J., Xia, X., 2015. Petrogenesis of the Early Cretaceous Laguila bimodal intrusive rocks from the Tethyan Himalaya: Implications for the break-up of Eastern Gondwana. Lithos 236–237, 190–202. https://doi.org/10.1016/j.lithos.2015.09.006
85. Marques, L.S., Dupré, B., Piccirillo, E.M., 1999. Mantle source compositions of the Parana Magmatic Province (southern Brazil): Evidence from trace element and Sr-Nd-

Pb isotope geochemistry. J. Geodyn. 28, 439–458. https://doi.org/10.1016/S0264-3707(99)00020-4

86. Marques, L.S., De Min, A., Rocha-Júnior, E.R.V., Babinski, M., Bellieni, G., Figueiredo, A.M.G., 2018. Elemental and Sr-Nd-Pb isotope geochemistry of the Florianópolis Dyke Swarm (Paraná Magmatic Province): crustal contamination and mantle source constraints. J. Volcanol. Geotherm. Res. 355, 149–164. https://doi.org/10.1016/j.jvolgeores.2017.07.005
87. Martinez, M., Deconinck, J.F., Pellenard, P., Riquier, L., Company, M., Reboulet, S., Moiroud, M., 2015. Astrochronology of the Valanginian-Hauterivian stages (Early Cretaceous): Chronological relationships between the Paraná-Etendeka large igneous province and the Weissert and the Faraoni events. Glob. Planet. Change 131, 158–173. https://doi.org/10.1016/j.gloplacha.2015.06.001
88. Mattioli, E., Pittet, B., Riquier, L., Grossi, V., 2014. The mid-Valanginian Weissert Event as recorded by calcareous nannoplankton in the Vocontian Basin. Palaeogeogr. Palaeoclimatol. Palaeoecol. 414, 472–485. https://doi.org/10.1016/j.palaeo.2014.09.030
89. McArthur, J.M., Janssen, N.M.M., Reboulet, S., Leng, M.J., Thirlwall, M.F., van de Schootbrugge, B., 2007. Palaeotemperatures, polar ice-volume, and isotope stratigraphy (Mg/Ca, δ18O, δ13C,87Sr/86Sr): The Early Cretaceous (Berriasian, Valanginian, Hauterivian). Palaeogeogr. Palaeoclimatol. Palaeoecol. 248, 391–430. https://doi.org/10.1016/j.palaeo.2006.12.015
90. Meyer, I., Davies, G.R., Stuut, J.B.W., 2011. Grain size control on Sr-Nd isotope provenance studies and impact on paleoclimate reconstructions: An example from deep-sea sediments offshore NW Africa. Geochemistry, Geophys. Geosystems 12. https://doi.org/10.1029/2010GC003355

91. Mingram, B., Trumbull, R.B., Littman, S., Gerstenberger, H., 2000. A petrogenetic study of anorogenic felsic magmatism in the Cretaceous Paresis ring complex, Namibia: Evidence for mixing of crust and mantle-derived components. Lithos 54, 1–22. https://doi.org/10.1016/S0024-4937(00)00033-5

92. Montero, P., Haissen, F., El Archi, A., Rjimati, E., Bea, F., 2014. Timing of Archean crust formation and cratonization in the Awsard-Tichla zone of the NW Reguibat Rise, West African Craton: A SHRIMP, Nd-Sr isotopes, and geochemical reconnaissance study. Precambrian Res. 242, 112–137. https://doi.org/10.1016/j.precamres.2013.12.013

93. Morales, C., Kujau, A., Heimhofer, U., Mutterlose, J., Spangenberg, J.E., Adatte, T., Ploch, I., Föllmi, K.B., 2015. Palaeoclimate and palaeoenvironmental changes through the onset of the Valanginian carbon-isotope excursion: Evidence from the Polish Basin. Palaeogeogr. Palaeoclimatol. Palaeoecol. 426, 183–198. https://doi.org/10.1016/j.palaeo.2015.03.013

94. O'Nions, R.K., Carter, S.R., Evensen, N.M., Hamilton, P.J., 1979. Geochemical and cosmochemical applications of Nd isotope analysis. Annu. Rev. earth Planet. Sci. Vol. 7 79, 11–38. https://doi.org/10.1146/annurev.ea.07.050179.000303

95. Ouajhain, B., Daoudi, L., Medina, F., Rocha, F., 2009. Contrôle paléogéographique de la sédimentation argileuse du Jurassique du bassin atlasique d'Essaouira (haut atlas occidental, Maroc). Comun. Geol. 96, 51–66.

96. Patchett, P.J., White, W.M., Feldmann, H., Kielinczuk, S., Hofmann, A.W., 1984. Hafnium/rare earth element fractionation in the sedimentary system and crustal recycling into the Earth's mantle. Earth Planet. Sci. Lett. 69, 365–378. https://doi.org/10.1016/0012-821X(84)90195-X

97. Pawlig, S., Gueye, M., Klischies, R., Schwarz, S., Wemmer, K., Siegesmund, S.,

2006. Geochemical and Sr-Nd isotopic data on the Birimian of the Kedougou-Kenieba Inlier (Eastern Senegal): Implications on the Palaeoproterozoic evolution of the West African Craton. South African J. Geol. 109, 411–427. https://doi.org/10.2113/gssajg.109.3.411

98. Peate, D.W., Hawkesworth, C.J., 1996. Lithospheric to asthenospheric transition in low-Ti flood basalts from southern Paraná, Brazil. Chem. Geol. 127, 1–24. https://doi.org/10.1016/0009-2541(95)00086-0

99. Peate, D.W., Hawkesworth, C.J., Mantovani, M.M.S., Rogers, N.W., Turner, S.P., 1999. Petrogenesis and stratigraphy of the high-Ti/Y Urubici magma type in the Parana Flood Basalt Province and implications for the nature of 'Dupal'-type mantle in the South Atlantic Region. J. Petrol. 40, 451–473. https://doi.org/10.1093/petroj/40.3.451

100. Peate, D.W., 2009. Global dispersal of Pb by large-volume silicic eruptions in the Paraná-Etendeka large igneous province. Geology 37, 1071–1074. https://doi.org/10.1130/G30338A.1

101. Peucat, J.J., Capdevila, R., Drareni, A., Choukroune, P., Fanning, C.M., Bernard-Griffiths, J., Fourcade, S., 1996. Major and trace element geochemistry and isotope (Sr, Nd, Pb, O) systematics of an Archaean basement involved in a 2.0 Ga very high-temperature (1000 °C) metamorphic event: In Ouzzal Massif, Hoggar, Algeria. J. Metamorph. Geol. 14, 667–692. https://doi.org/10.1111/j.1525-1314.1996.00054.x

102. Peucat, J.J., Capdevila, R., Drareni, A., Mahdjoub, Y. and Kahoui, M., 2005. The Eglab massif in the West African Craton (Algeria), an original segment of the Eburnean orogenic belt: petrology, geochemistry and geochronology. Precambrian Research, 136(3-4), 309-352

103. Piqué, A., Le Roy, P., Amrhar, M., 1998. Transtensive synsedimentary tectonics associated with ocean opening: The Essaouira-Agadir segment of the Moroccan Atlantic margin. J. Geol. Soc. London. 155, 913–928. https://doi.org/10.1144/gsjgs.155.6.0913

104. Plank, T., Ludden, J.N., 1992. Geochemistry of sediments in the Argo Abyssal Plain at Site 765: a continental margin reference section for sediment recycling in subduction zones. Proc., Sci. results, ODP, Leg 123, Argo Abyssal Plain/Exmouth Plateau. https://doi.org/10.2973/odp.proc.sr.123.158.1992

105. Plank, T., Ludden, J.N., Escutia, C., 2000. Site 1149. Proc. Ocean Drill. Program, 185 Initial Reports 185, 1–190. https://doi.org/10.2973/odp.proc.ir.185.104.2000

106. Plank, T., Kelley, K.A., Murray, R.W., Stern, L.Q., 2007. Chemical composition of sediments subducting at the Izu-Bonin trench. Geochemistry, Geophys. Geosystems 8, 1–16. https://doi.org/10.1029/2006GC001444

107. Poulsen, C.J., Seidov, D., Barron, E.J., Peterson, W.H., 1998. The impact of paleogeographic evolution on the surface oceanic circulation and the marine environment within the mid-Cretaceous Tethys. Paleoceanography 13, 546–559. https://doi.org/10.1029/98PA01789

108. Price, G.D., Sellwood, B.W., Valdes, P.J., 1995. Sedimentological evaluation of general circulation model simulations for the “greenhouse” Earth: Cretaceous and Jurassic case studies. Sediment. Geol. 100, 159–180. https://doi.org/10.1016/0037-0738(95)00106-9

109. Price, G.D., Mutterlose, J., 2004. Isotopic signals from late Jurassic-early Cretaceous (Volgian-Valanginian) sub-Arctic belemnites, Yatria River, Western Siberia. J. Geol. Soc. London. 161, 959–968. https://doi.org/10.1144/0016-764903-

110. Price, G.D., Janssen, N.M.M., Martinez, M., Company, M., Vandevelde, J.H., Grimes, S.T., 2018. A High-Resolution Belemnite Geochemical Analysis of Early Cretaceous (Valanginian-Hauterivian) Environmental and Climatic Perturbations. Geochemistry, Geophys. Geosystems 19, 3832–3843. https://doi.org/10.1029/2018GC007676

111. Rämö, O.T., Heikkilä, P.A., Pulkkinen, A.H., 2016. Geochemistry of Paraná-Etendeka basalts from Misiones, Argentina: Some new insights into the petrogenesis of high-Ti continental flood basalts. J. South Am. Earth Sci. 67, 25–39. https://doi.org/10.1016/j.jsames.2016.01.008

112. Reboulet, S., Mattioli, E., Pittet, B., Baudin, F., Olivero, D., Proux, O., 2003. Ammonoid and nannoplankton abundance in Valanginian (early Cretaceous) limestone-marl successions from the southeast France Basin: Carbonate dilution or productivity? Palaeogeogr. Palaeoclimatol. Palaeoecol. 201, 113–139. https://doi.org/10.1016/S0031-0182(03)00541-8

113. Reboulet, S., Jaillard, E., Shmeit, M., Giraud, F., Masrour, M. and Spangenberg, J.E., 2022. Biostratigraphy, carbon isotope and sequence stratigraphy of South Tethyan Valanginian successions in the Essaouira-Agadir Basin (Morocco). Cretac. Res. 140, 105341. https://doi.org/10.1016/j.cretres.2022.105341

114. Rocha-Júnior, E.R.V., Marques, L.S., Babinski, M., Nardy, A.J.R., Figueiredo, A.M.G., Machado, F.B., 2013. Sr-Nd-Pb isotopic constraints on the nature of the mantle sources involved in the genesis of the high-Ti tholeiites from northern Paraná Continental Flood Basalts (Brazil). J. South Am. Earth Sci. 46, 9–25. https://doi.org/10.1016/j.jsames.2013.04.004

115. Rocha, B.C., Janasi, V.A., Polo, L.A., Rocha, B.C., Davies, J.H.F.L.,

Schaltegger, U., Greber, N.D., Davies, J.H.F.L., Nardy, A.J.R., Lucchetti, A.C.F., Greber, N.D., 2020. Rapid eruption of silicic magmas from the Paraná magmatic province (Brazil) did not trigger the Valanginian event. Geology 48, 1174–1178. https://doi.org/10.1130/G47766.1

116. Rudnick, R.L., Gao, S., 2013. Composition of the Continental Crust. Treatise Geochemistry Second Ed. 4, 1–51. https://doi.org/10.1016/B978-0-08-095975-7.00301-6

117. Sauzéat, L., Rudnick, R.L., Chauvel, C., Garçon, M., Tang, M., 2015. New perspectives on the Li isotopic composition of the upper continental crust and its weathering signature. Earth Planet. Sci. Lett. 428, 181–192. https://doi.org/10.1016/j.epsl.2015.07.032

118. Schlanger, S.O., Jenkyns, H.C., 1976. Cretaceous Oceanic Anoxic Events: Causes and Consequences.

119. Scholle, P.A., Arthur, M.A., 1980. Carbon isotope fluctuations in Cretaceous pelagic limestones: potential stratigraphic and petroleum exploration tool. Am. Assoc. Pet. Geol. Bull. 64, 67–87. https://doi.org/10.1306/2F91892D-16CE-11D7-8645000102C1865D

120. Scotese C.R., 2016. PALEOMAP PaleoAtlas for GPlates and the PaleoData Plotter Program, PALEOMAP Project. http://www.scotese.com

121. Shmeit, M., F. Giraud, E. Jaillard, S. Reboulet, M. Masrour, J. E. Spangenberg, and A. El-Samrani., 2022. The Valanginian Weissert Event on the south Tethyan margin: A dynamic paleoceanographic evolution based on the study of calcareous nannofossils. Marine Micropaleontology 102134. https://doi.org/10.1016/j.marmicro.2022.102134

122. Skonieczny, C., Bory, A., Bout-Roumazeilles, V., Abouchami, W., Galer,

S.J.G., Crosta, X., Diallo, A., Ndiaye, T., 2013. A three-year time series of mineral dust deposits on the West African margin: Sedimentological and geochemical signatures and implications for interpretation of marine paleo-dust records. Earth Planet. Sci. Lett. 364, 145–156. https://doi.org/10.1016/j.epsl.2012.12.039

123. Sprovieri, M., Coccioni, R., Lirer, F., Pelosi, N., Lozar, F., 2006. Orbital tuning of a lower Cretaceous composite record (Maiolica Formation, central Italy). Paleoceanography 21. https://doi.org/10.1029/2005PA001224

124. Tapsoba, B., Lo, C.H., Jahn, B.M., Chung, S.L., Wenmenga, U., Iizuka, Y., 2013. Chemical and Sr-Nd isotopic compositions and zircon U-Pb ages of the Birimian granitoids from NE Burkina Faso, West African Craton: Implications on the geodynamic setting and crustal evolution. Precambrian Res. 224, 364–396. https://doi.org/10.1016/j.precamres.2012.09.013

125. Thirlwall, M.F., 1991. Long-term reproducibility of multicollector Sr and Nd isotope ratio analysis. Chem. Geol. 94, 85–104. https://doi.org/10.1016/S0009-2541(10)80021-X

126. Thompson, R.N., Gibson, S.A., Dickin, A.P., Smith, P.M., 2001. Early cretaceous basalt and picrite dykes of the Southern Etendeka Region, NW Namibia: Windows into the role of the Tristan mantle plume in Paraná-Etendeka magmatism. J. Petrol. 42, 2049–2081. https://doi.org/10.1093/petrology/42.11.2049

127. Toummite, A., Liegeois, J.P., Gasquet, D., Bruguier, O., Beraaouz, E.H., Ikenne, M., 2013. Field, geochemistry and Sr-Nd isotopes of the Pan-African granitoids from the Tifnoute Valley (Sirwa, Anti-Atlas, Morocco): A post-collisional event in a metacratonic setting. Mineral. Petrol. 107, 739–763. https://doi.org/10.1007/s00710-012-0245-3

128. Trumbull, R.B., Harris, C., Frindt, S., Wigand, M., 2004. Oxygen and

neodymium isotope evidence for source diversity in Cretaceous anorogenic granites from Namibia and implications for A-type granite genesis. Lithos 73, 21–40. https://doi.org/10.1016/j.lithos.2003.10.006

129. Turner, S.P., Kirstein, L.A., Hawkesworth, C.J., Peate, D.W., Hallinan, S., Mantovani, M.S.M., 1999. Petrogenesis of an 800 m lava sequence in eastern Uruguay: Insights into magma chamber processes beneath the Parana flood basalt province. J. Geodyn. 28, 471–487. https://doi.org/10.1016/S0264-3707(99)00022-8

130. Van De Schootbrugge, B., Kuhn, O., Adatte, T., Steinmann, P., Föllmi, K., 2003. Decoupling of P- And Corg-burial following Early Cretaceous (Valanginian-Hauterivian) platform drowning along the NW Tethyan margin. Palaeogeogr. Palaeoclimatol. Palaeoecol. 199, 315–331. https://doi.org/10.1016/S0031-0182(03)00540-6

131. Villa, I.M., De Bièvre, P., Holden, N.E., Renne, P.R., 2015. IUPAC-IUGS recommendation on the half life of 87Rb. Geochim. Cosmochim. Acta 164, 382–385. https://doi.org/10.1016/j.gca.2015.05.025

132. Villa, I.M., Holden, N.E., Possolo, A., Ickert, R.B., Hibbert, D.B. and Renne, P.R., 2020. IUPAC-IUGS recommendation on the half-lives of ^{147}Sm and ^{146}Sm. Geochimica et cosmochimica acta, 285, 70-77. https://doi.org/10.1016/j.gca.2020.06.022

133. Weissert, H., 1989. C-Isotope stratigraphy, a monitor of paleoenvironmental change: A case study from the early cretaceous. Surv. Geophys. 10, 1–61. https://doi.org/10.1007/BF01901664

134. Weissert, H., Lini, A., Föllmi, K.B., Kuhn, O., 1998. Correlation of Early Cretaceous carbon isotope stratigraphy and platform drowning events: A possible link? Palaeogeogr. Palaeoclimatol. Palaeoecol. 137, 189–203.

https://doi.org/10.1016/S0031-0182(97)00109-0

135. Westermann, S., Föllmi, K.B., Adatte, T., Matera, V., Schnyder, J., Fleitmann, D., Fiet, N., Ploch, I., Duchamp-Alphonse, S., 2010. The Valanginian δ13C excursion may not be an expression of a global oceanic anoxic event. Earth Planet. Sci. Lett. 290, 118–131. https://doi.org/10.1016/j.epsl.2009.12.011

136. Westermann, S., Duchamp-Alphonse, S., Fiet, N., Fleitmann, D., Matera, V., Adatte, T., Föllmi, K.B., 2013. Paleoenvironmental changes during the valanginian: New insights from variations in phosphorus contents and bulk- and clay mineralogies in the western tethys. Palaeogeogr. Palaeoclimatol. Palaeoecol. 392, 196–208. https://doi.org/10.1016/j.palaeo.2013.09.017

137. White, W.M., Albarède, F., Télouk, P., 2000. High-precision analysis of Pb isotope ratios by multi-collector ICP-MS. Chem. Geol. 167, 257–270. https://doi.org/10.1016/S0009-2541(99)00182-5

138. Wortmann, U.G., Weissert, H., 2000. Tying platform drowning to perturbations of the global carbon cycle with a delta d13COrg-curve from the Valanginian of DSDP Site 416. Terra Nov. 12, 289–294. https://doi.org/10.1046/j.1365-3121.2000.00312.x

139. Zhu, D., Mo, X., Pan, G., Zhao, Z., Dong, G., Shi, Y., Liao, Z., Wang, L., Zhou, C., 2008. Petrogenesis of the earliest Early Cretaceous mafic rocks from the Cona area of the eastern Tethyan Himalaya in south Tibet: Interaction between the incubating Kerguelen plume and the eastern Greater India lithosphere? Lithos 100, 147–173. https://doi.org/10.1016/j.lithos.2007.06.024

140. Zhu, D., Chung, S.L., Mo, X.X., Zhao, Z.D., Niu, Y., Song, B., Yang, Y.H., 2009. The 132 Ma Comei-Bunbury large igneous province: Remnants identified in present-day southeastern Tibet and southwestern Australia. Geology 37, 583–586.

https://doi.org/10.1130/G30001A.1

Figure captions

Fig. 1. Location of the study area in SW Morocco, modified from Ouajhain et al. (2009). (a) Location of the central Moroccan margin including the Essaouira-Agadir Basin and DSDP Hole 416A (star shape–not to scale). (b) Geological sketch including the location of the Zalidou section (star shape)

Fig. 2. Palaeogeographic map of the Valanginian (~135 Ma) showing the approximate location of the central Moroccan margin (star shape). The "red masses" correspond to the approximate locations of the Valanginian large igneous provinces (LIPs). Construction from Scotese (2016) PaleoAtlas

Fig. 3. a) SiO_2 and b) CaO *vs.* Al_2O_3 contents (wt %) in Zalidou and Hole 416A plotted before, during and after the Weissert Event. Also, data points are shown from Plank et al. (2007) for Site 1149, Plank and Ludden (1992) for Site 765 and Carpentier et al. (2009) for Sites 144 and 543

Fig. 4. Stratigraphic variations of selected major and trace elements in Zalidou and Hole 416A. Also plotted, the $\delta^{13}C_{carb}$ from Shmeit et al. (2022). The colored interval (green) corresponds to the Weissert Event following Shmeit et al. (2022). For more information on the litho- and bio-stratigraphy see caption of Fig. S2. CIA: chemical index of alteration, defined as the molar ratio of $[Al_2O_3/(Al_2O_3+CaO^*+Na_2O+K_2O)]\times100$, with CaO* representing CaO in silicate minerals only

Fig. 5. Comparison of trace elements between Zalidou and Hole 416A. Data points are shown from Plank et al. (2007) for Site 1149, Plank and Ludden (1992) for Site 765 and Carpentier et al. (2009) for Sites 144 and 543

Fig. 6. Stratigraphic variations in measured and initial isotope ratios of Pb, Sr and Nd in Zalidou and Hole 416A (see Supplementary Table). Error bars on measured isotopic ratios are assessed from analytical measurements of the international reference materials. The colored interval (green) corresponds to the Weissert Event following Shmeit et al. (2022); see also caption of Fig. S2. Initial isotope ratios are calculated at 135 Ma using the decay constants and the half-life of parent/daughter decay systems from Villa et al. (2015) for Rb-Sr, Jaffey et al. (1971) and Le Roux and Glendenin (1963) for U-Th-Pb, and Villa et al. (2020) for Sm-Nd

Fig. 7. Comparing the initial (i) isotope ratios at 135 Ma of Pb, Sr and Nd between Zalidou and Hole 416A sediments

Fig. 8. Comparing the initial isotope ratios at 135 Ma of the central Moroccan margin sediments with Early Cretaceous large igneous provinces (LIPs). References of the isotope ratios for LIPs (see also Supplementary Table): Paraná basalts (Hawkesworth et al., 1986; Peate and Hawkesworth, 1996; Peate et al., 1999; Turner et al., 1999; Rocha-Júnior et al., 2013; Barreto et al., 2016; Rämö et al., 2016; Marques et al., 1999; 2018), Etendeka basalts (Ewart et al., 1998a, 2004a; Le Roex and Lanyon, 1998; Mingram et al., 2000; Thompson et al., 2001), Etendeka silicic sequences (Ewart et al., 1998b, 2004b; Trumbull et al., 2004), Comei basalts (Zhu et al., 2008; Liu et al., 2015) and the Bunbury basalt and silicic sequences (Ewart et al., 1992; Frey et al., 1996; Allen et al., 1997; Direen et al., 2017)

Fig. 9. Comparing initial isotope ratios of the central Moroccan margin sediments with surrounding possible source areas having only Sr and Nd isotopes. Green-scale: Moroccan massifs; yellow-scale: African and Saharan dust sources; and purple-scale: West African Craton. Data references (see also Supplementary Table): Central Jebilet 240-330 Ma (Essaifi et al., 2014; Bouloton et al., 2019), Anti-Atlas 543-560 Ma (Toummite et al., 2013; Belkacim et al., 2017), Central High Atlas 165-125 Ma (Essaifi and Zayane, 2018), Western High Atlas

290 Ma (Gasquet et al., 1992), NE Meseta 344 Ma (Ajaji et al., 1998) and east Moroco complex including the El Jadida complex (Chalot-Prat, 1995; Gasquet et al., 2005; EL Haibi et al., 2020); Holocene Peri-Saharan dust (Grousset et al., 1992), modern African and Saharan dust (Grousset and Biscaye, 2005; Skonieczny et al., 2013; Gross et al., 2016), modern Sahel desert dusts (Kumar et al., 2014), modern along with Holocene subtropical Saharan/Atlantic sediments (Grousset et al., 1998; Meyer et al., 2011) and the central Sahara Bodélé Depression (Abouchami et al., 2013); and WAC (West African Craton) 2.1 Ga (Boher et al., 1992; Pawlig et al., 2006; Tapsoba et al., 2013), 2.9 Ga WAC and Reguibat Rise (Blanc et al., 1992; Peucat et al., 1996; 2005; Bea et al., 2013; Montero et al., 2014) and 900 Ma Saharan metacraton (Küster et al., 2008)

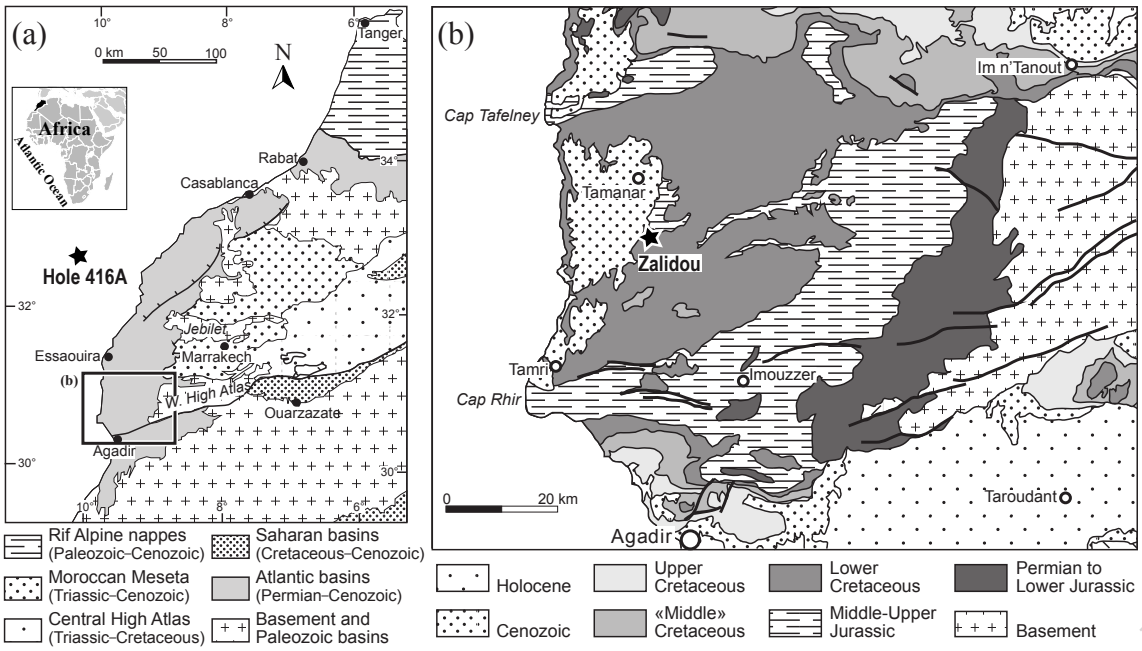

Figure 1

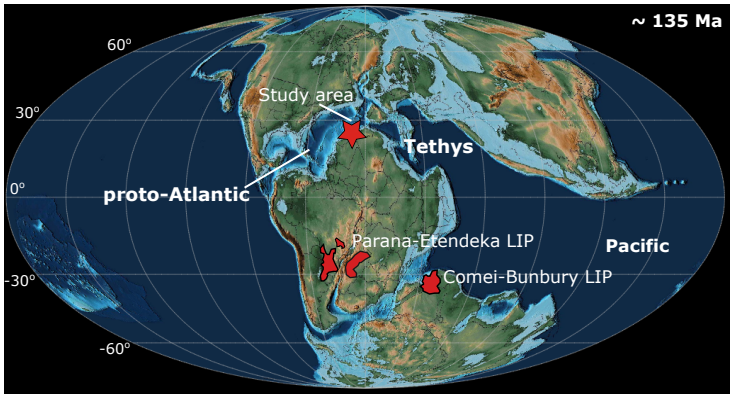

Figure 2

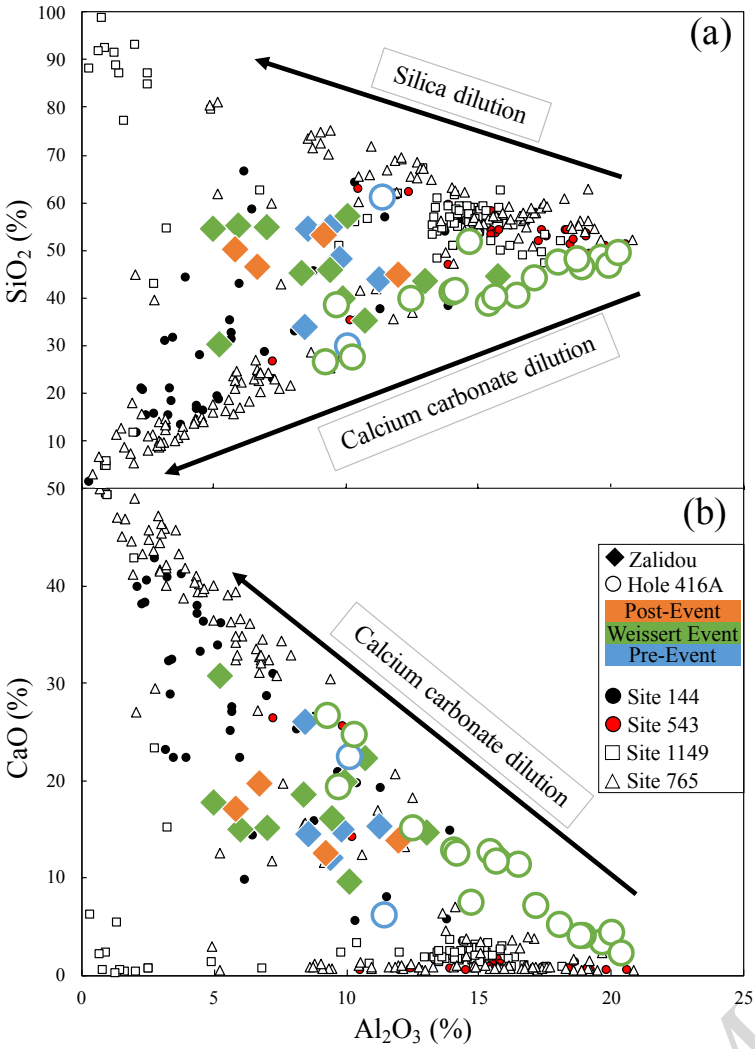

Figure 3

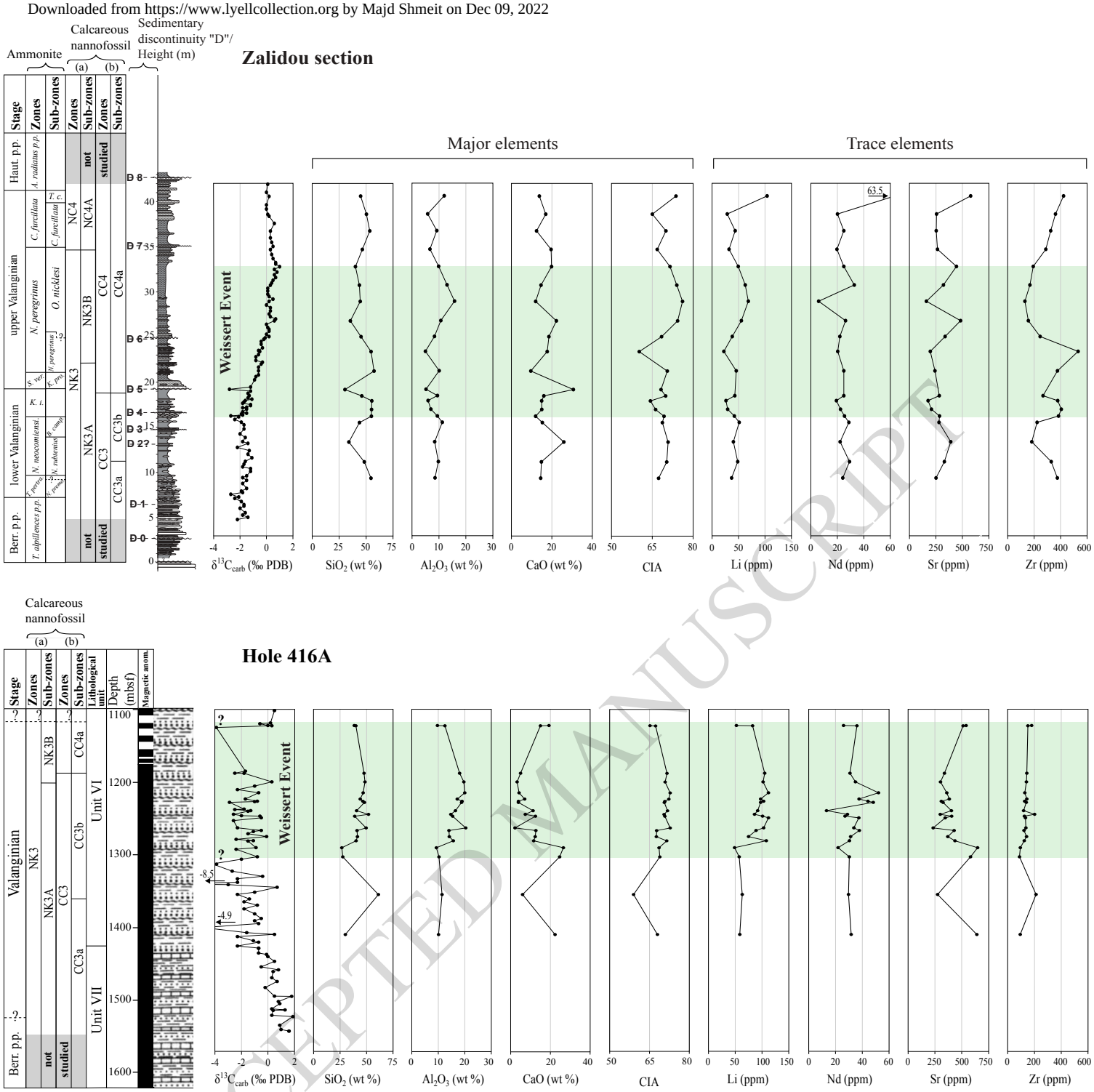

Figure 4

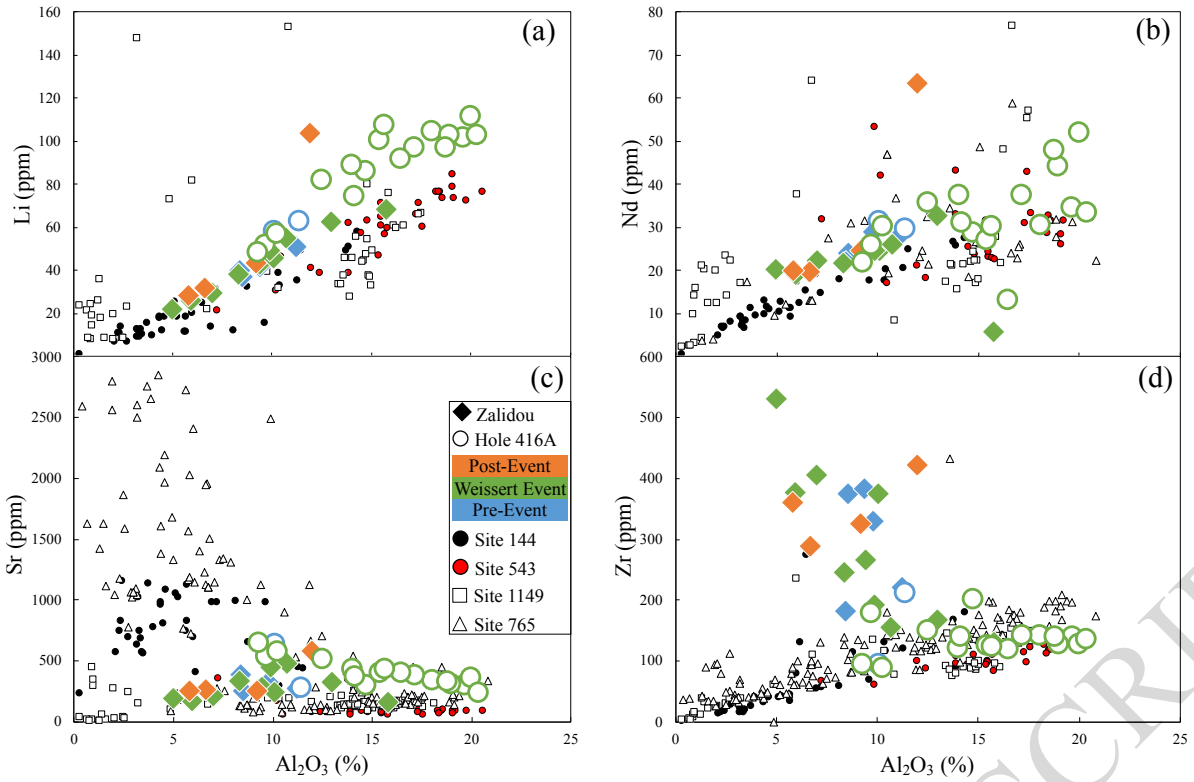

Figure 5

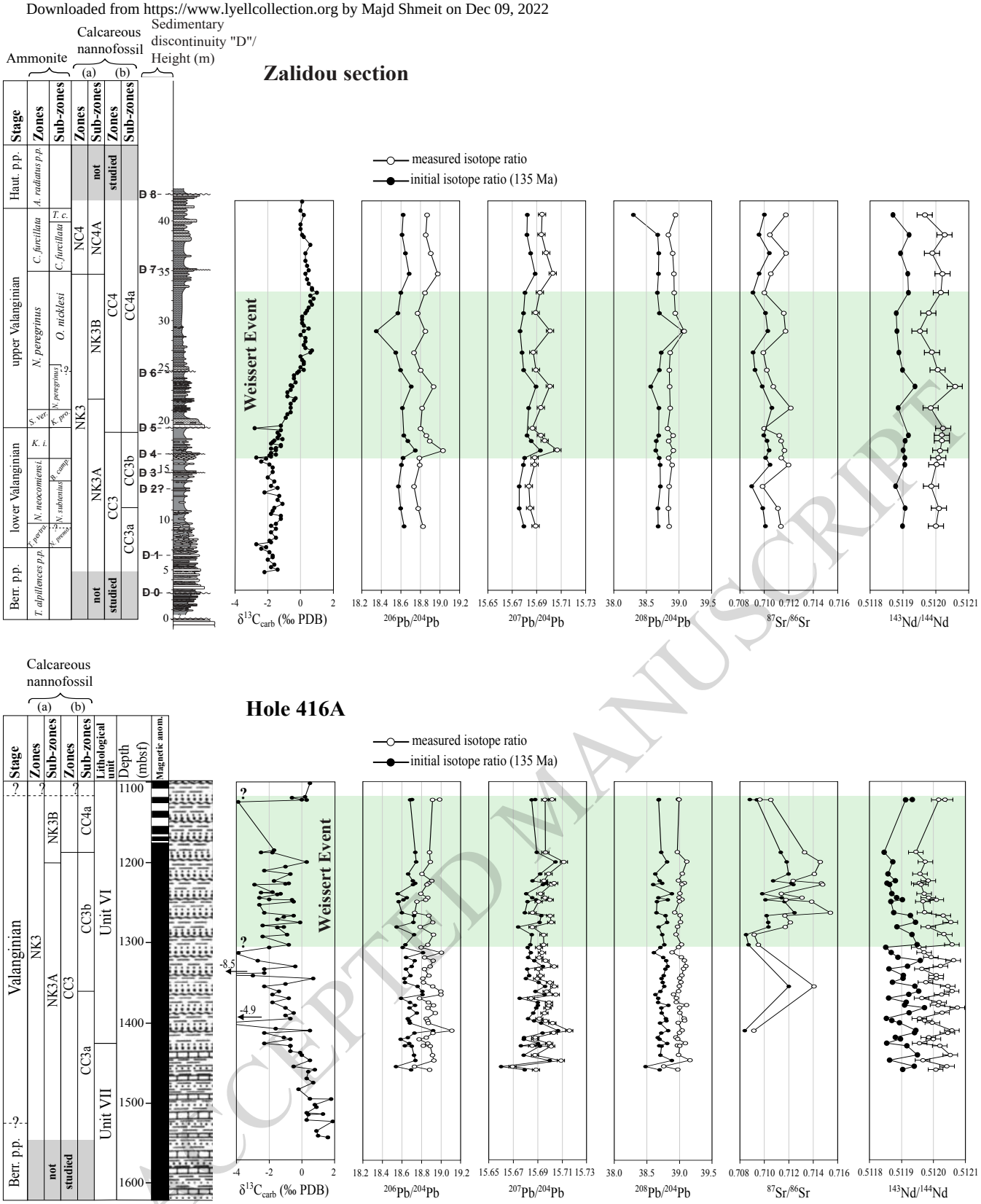

Figure 6

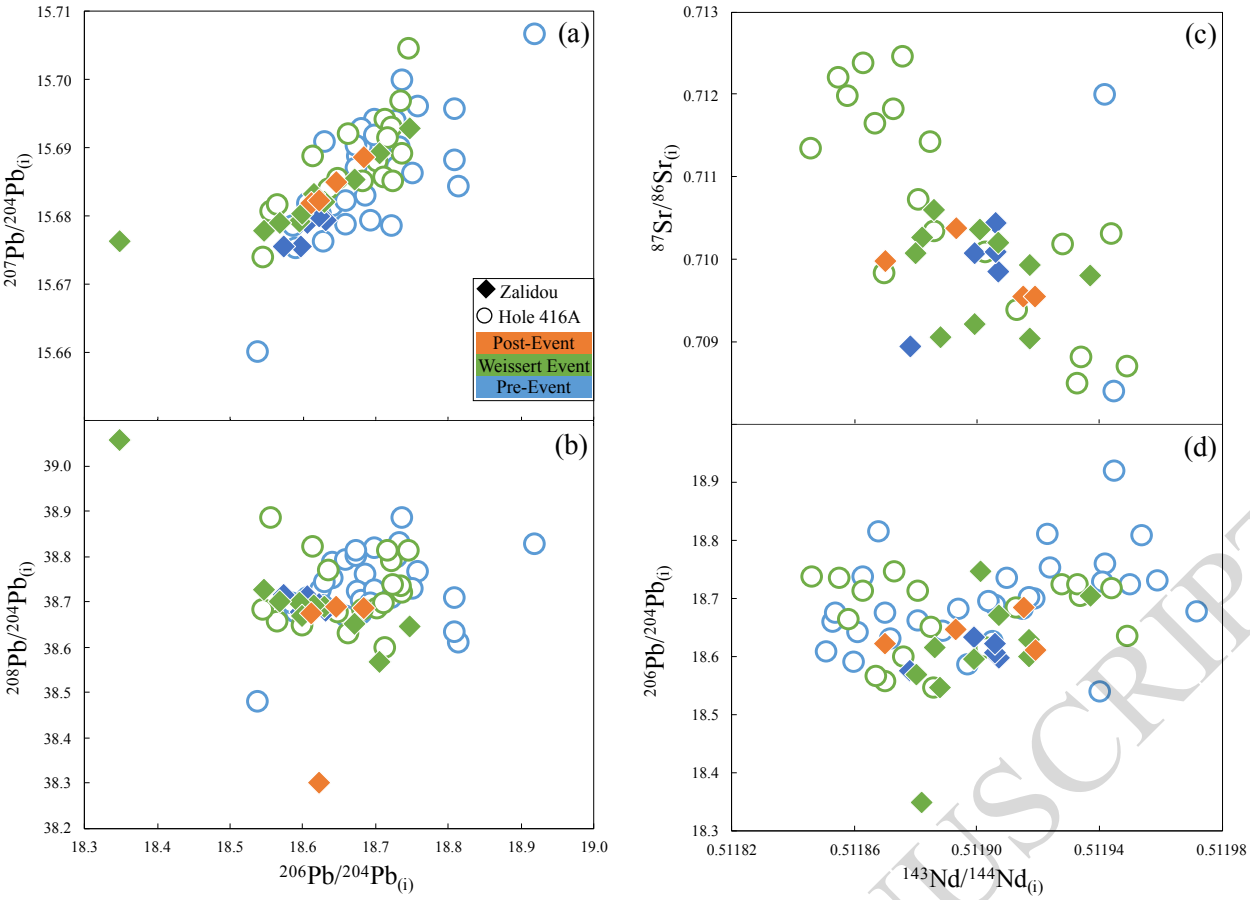

Figure 7

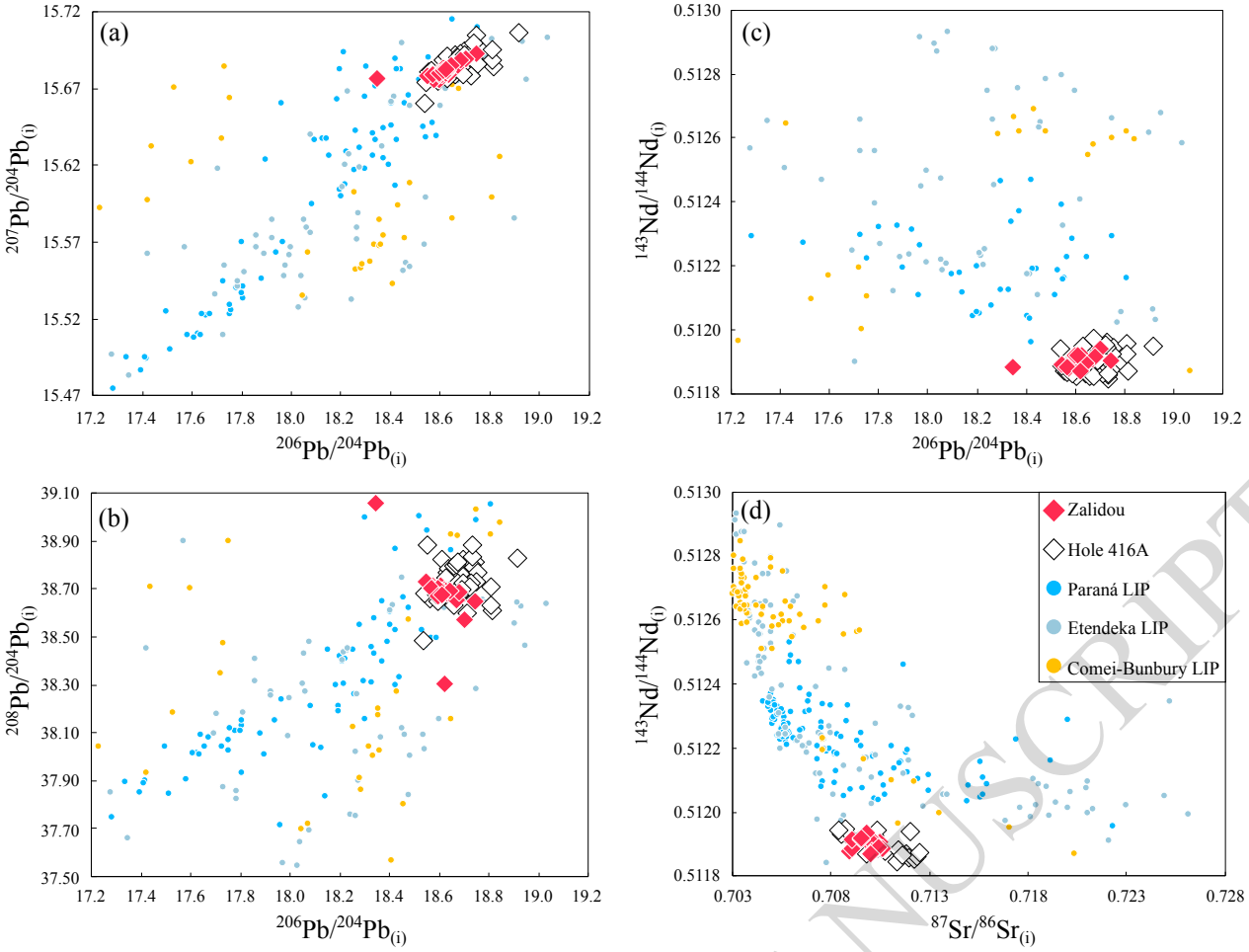

Figure 8

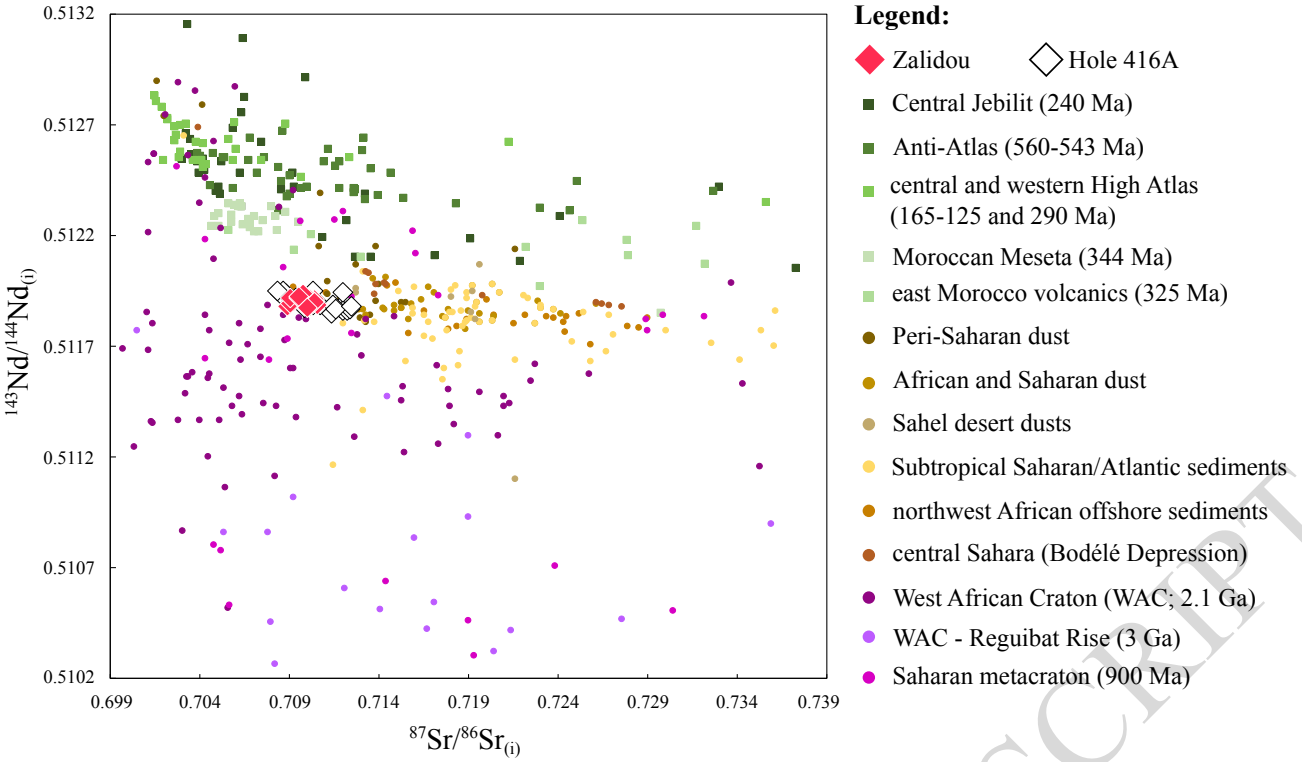

Figure 9